Quaternary Science Advances 15 (2024) 100223

Contents lists available at ScienceDirect

Quaternary Science Advances

journal homepage: www.sciencedirect.com/journal/quaternary-science-advances

Changes in the particulate organic carbon pump efficiency since the Last Glacial Maximum in the northwestern Philippine Sea

Pierrick Fenies [a,b,*], Maria-Angela Bassetti [a], Natalia Vazquez Riveiros [c], Sze Ling Ho [b], Yuan-Pin Chang [d], Ludvig Löwemark [e], Florian Bretonnière [a,f], Nathalie Babonneau [c], Gueorgui Ratzov [f], Shu-Kun Hsu [g,h], Chih-Chieh Su [b]

[a] CEFREM-UMR 5110, Université de Perpignan Via Domitia, UMR 5110, Perpignan, 66860, France
[b] Institute of Oceanography, National Taiwan University, No. 1, Sec. 4, Roosevelt Road, 10617 Taipei, Taiwan
[c] Geo-Ocean, UMR 6538, CNRS-Ifremer-UBO-UBS, Plouzané, France
[d] Institute of Marine Geology and Chemistry, National Sun Yat-sen University, Kaohsiung, Taiwan
[e] Department of Geosciences, National Taiwan University, No 1. Sec. 4 Roosevelt Road, Taipei, 106, Taiwan
[f] Université Côte d'Azur, CNRS, Observatoire de la Côte d'Azur, IRD, Géoazur, Nice, France
[g] Department of Earth Sciences, National Central University, Taoyuan, 32001, Taiwan
[h] Institute of Earth Sciences, Academia Sinica, Taipei, 11529, Taiwan

ARTICLE INFO

Keywords:
Bottom
Pore water oxygenation
Paleoproductivity
Typhoon
Benthic foraminifera
Monsoon
Turbidity pump
Marine biological pump

ABSTRACT

Changes in bottom and pore water oxygenation over glacial – interglacial cycles have influenced the ocean's capacity to store particulate organic carbon regardless of its source, either the marine primary productivity or the continent-to-ocean transfer of terrestrial organic matter. In the Philippine Sea, east off Taiwan, despite being currently oligotrophic, the enhanced East Asian Winter Monsoon during the Last Glacial Maximum and the Heinrich Stadial 1 might have altered the nutrient budget in surface waters by providing nutrients from the Eurasian loess dust and deepening the vertical mixing, bringing nutrients from the nutrient-enriched Kuroshio Current subsurface waters to the surface. During the deglaciation, previous studies also suggest an overall weakening of the marine biological pump during the Heinrich Stadial 1, and the rise in sea level is expected to have led to a global significant decline in the ability of continents to bury their particulate organic carbon in marine sediments. However, changes in the continent-ocean transfer of terrestrial organic matter and on the marine biological pump around Taiwan remain poorly constrained.

In the present study, we have thus aimed to reconstruct bottom – pore water oxygenation, past marine primary productivity and continental-ocean transfer of terrestrial particulate organic carbon to the ocean since the end of the Last Glacial Maximum, in order to better constrain the ability of marine sediments to capture atmospheric carbon over the past 20,000 years. To this end, sediment core MD18-3523 has been recovered from a levee of Hoping Canyon, north-east of Taiwan, in the Ryukyu forearc basin. The reconstructions were made possible by the application of multivariate statistics and transfer functions on benthic foraminiferal assemblages, by the measurement of total organic carbon concentration and by the investigation of chemical element ratios obtained from X-ray fluorescence (XRF).

We observed a transition across the Bølling–Allerød and the Younger Dryas from suboxic-dysoxic bottom – pore waters during Heinrich Stadial 1 to oxic-suboxic during the Holocene, and revealed an increase in marine primary productivity during Heinrich Stadial 1 in all probability due to intensified East Asian Winter Monsoon winds. We have also identified periods of enhanced terrestrial particulate organic carbon transfer to the ocean driven by short-lived extreme events, most likely typhoons, during the Bølling–Allerød, at the beginning of the Early Holocene and the end of the Late Holocene, when the typhoon dynamics affecting Taiwan were intensified. Overall, these findings suggest an enhanced marine biological pump during the Heinrich Stadial 1 and an efficient carbon turbidity pump during the Bølling–Allerød, the Early and Late Holocene, contrasting with the western coast of Taiwan.

* Corresponding author. CEFREM-UMR 5110, Université de Perpignan Via Domitia, UMR 5110, Perpignan, 66860, France.
E-mail address: pie.fenies@gmail.com (P. Fenies).

https://doi.org/10.1016/j.qsa.2024.100223
Received 27 December 2023; Received in revised form 16 July 2024; Accepted 18 July 2024
Available online 28 July 2024

1. Introduction

The carbon cycle represents the transfer of dissolved and particulate carbon between the Earth's various inventories. On the glacial-interglacial scale, the ocean plays a central role as the largest carbon reservoir capable of rapidly (on decadal to millennial timescales) sequestering atmospheric and terrestrial carbon and transferring the carbon it contains to the atmosphere (Bauer et al., 2013; DeVries, 2022; Talling et al., 2024). A proportion of the particulate organic carbon is designated as biospheric in that it originates from the capture of atmospheric carbon during terrestrial or marine photosynthesis. Consequently, alterations in the burial of this biospheric particulate organic carbon in marine sediments would result in changes in atmospheric CO2 concentration (Cartapanis et al., 2016; DeVries, 2022; Hilton, 2017; Hilton et al., 2008, 2012; Jørgensen et al., 2022; Talling et al., 2024). Two main mechanisms enable the effective burial of biospheric particulate organic carbon in marine sediments: the transfer of terrestrial particulate organic carbon by turbidity currents (Hilton, 2017; Hilton et al., 2008, 2012; Talling et al., 2024) and the sinking of particle organic carbon produced by the marine primary productivity (DeVries, 2022; Siegel et al., 2023). Together, this turbidity pump and this component of the marine biological pump, form the particulate organic carbon pump, and are currently estimated to be between 220 and 305 Mt C per year. Of this, 90 to 130 Mt C per year is attributable to the marine biological pump, and 103 to 138 Mt C per year – out of a total of 130–175 Mt C per year of total terrestrial particulate organic carbon transported to the ocean by rivers – is attributable to the turbidity pump (Talling et al., 2024). However, changes in the efficiency of these two separate mechanisms from the Last Glacial Maximum Maximum (LGM; 23.0–19.0 ka; Mix et al., 2001) to the Late Holocene (4.2–0.0 ka; Walker et al., 2012) are still poorly constrained at global and regional scale (Cartapanis et al., 2016; Talling et al., 2024).

The North Pacific Ocean is one of the largest reservoirs of marine carbon. This is partly because the Pacific Deep Water (PDW, 1000–4500 m water depth) marks the terminus of the oceanic overturning circulation in this region (Talley et al., 2011) and contains the highest concentration of dissolved organic carbon of any other oceans (Hansell et al., 2009). The lack of present-day deep water formation in the North Pacific leads to a reduction of PDW oxygenation due to pronounced stratification of the of the subarctic region (Ferreira et al., 2018; Warren, 1983). However, several studies have shown a considerably different Pacific Meridional Overturning Circulation (PMOC) from the LGM to the beginning of the Bølling-Allerød (BA; 14.7–12.9 ka; Clark et al., 2012) relative to its modern counterpart (Cook et al., 2016; Keigwin, 1998; Matsumoto et al., 2002; Okazaki et al., 2012; Rae et al., 2020; Rafter et al., 2022), with enhanced North Pacific Intermediate Water (NPIW; 500–1000 m water depth; Talley et al., 2011) formation in the Okhotsk and Bering Seas, notably during Heinrich Stadial 1 (HS1; 18.0–14.7 ka; Denton et al., 2010; Max et al., 2014; Ohkushi et al., 2013; Okazaki et al., 2014, 2010; Zou et al., 2020).

There is a consensus on the extension of NPIW to 2000 m water depth and an intensification of its ventilation and oxygenation during HS1 (Erdem et al., 2020; Ohkushi et al., 2013; Okazaki et al., 2012, 2014; Rafter et al., 2022; Zou et al., 2020). However, it remains uncertain whether this enhancement in oxygenation and ventilation has affected water masses beyond the 2000 m threshold. Some studies suggest an expansion down to ~ 3000 m depth (Horikawa et al., 2021; Keigwin and Lehman, 2015; Okazaki et al., 2010; Rae et al., 2014), while others advocate the existence of a stratification front at 2000 m, hindering the vertical diffusion of dissolved oxygen and the increase of the ventilation of the bottom layers (Gong et al., 2019; Jaccard and Galbraith, 2013; Okazaki et al., 2012; Rafter et al., 2022). The depth of this front directly affects the volume of oxygen-depleted bottom water and thus the efficiency of particulate organic carbon storage: the shallower the front, the more efficient the storage.

Fossil-based paleo-oxygenation records exist throughout the North Pacific that illustrate the evolution of PDW ventilation since the LGM (Belanger et al., 2020; Du et al., 2022; Jacobel et al., 2020; Ovsepyan et al., 2021; Sharon and Belanger, 2022). However, the deep water masses of the western subtropical North Pacific region have not been investigated intensively, the available studies focusing mainly on intermediate water (<2000 m) oxygenation changes in the partially enclosed Chinese coastal seas rather than on deep water (>2000 m) oxygenation in the unenclosed Philippine Sea, open to the North Pacific (Li et al., 2017, 2018, 2020; Lim et al., 2017; Vats et al., 2021; Zou et al., 2020, 2021). Regarding the transfer of particulate organic carbon in the Philippine Sea by the marine biological pump and the turbidity pump, recent studies have highlighted an enhanced primary productivity and continent – ocean supply of terrestrial carbon by rivers to the deep ocean during the LGM and the HS1 (Fenies et al., 2023; Xu et al., 2020). Low bottom – pore water oxygenation combined with intensified marine primary productivity and transfer of continental particulate organic carbon from the biosphere might result in the establishment of an enhanced particulate organic carbon pump in this region.

Therefore, in order to constrain the changes in the efficiency of the particulate organic carbon pump in the northwestern Philippine Sea, a multi-proxy study was performed on the sediment core MD18-3523 (Fig. 1) retrieved at ~3000 m depth, offshore northeastern Taiwan. The water depth of this site makes the sediment core an ideal archive to investigate the extent of the water depth affected by the intensified ventilation/oxygenation of NPIW, and its position on a levee of the Hoping Canyon enables investigation of the transfer of terrestrial particulate organic carbon by turbidity currents. Changes in bottom – pore water oxygenation were inferred using X-Ray Fluorescence (XRF) elemental ratio Mn/Fe on bulk sediment, benthic foraminifera assemblages and derived oxygen transfer functions; changes in marine primary productivity were reconstructed using Benthic Foraminifera Accumulation Rate (BFAR), XRF elemental ratio Br/Ti on bulk sediment and Total Organic Carbon (TOC) measurements; changes in continent-ocean transfer of terrestrial particulate organic carbon were reconstructed using sedimentation rate, XRF elemental ratios Ti/K and Br/Ti, benthic foraminifera assemblages, TOC and BFAR.

2. Regional setting

Taiwan is located between 21°54′N and 25°18′N along the Eurasian margin, in the north-western part of the Philippine Sea (Fig. 1a). The island is characterized by the high elevation of the north-south Central Range culminating at 3952 m. It is bisected by the Tropic of Cancer and presents an average annual temperature range from 22 °C in the north to 24 °C in the south. Due to the influence of the East Asian Summer Monsoon (EASM) and the occurrence of many typhoons (Chen and Chen, 2003), Taiwan is subject to intense rainfall, with 2500 mm yr^{-1} on average that can reach 5000 mm yr^{-1} in the north-east of the island (Li et al., 2013; Resentini et al., 2017).

High frequency of typhoons and earthquakes, landslide remobilization on high and steep reliefs (Dadson et al., 2003; Steer et al., 2020) and high rainfall intensity lead to an extremely high erosion rate of 3–6 mm yr^{-1} on average, reaching 60 mm yr^{-1} locally around the active thrust faults in the southwest (Derrieux et al., 2014). The narrowness (<3300 km^2) and steepness of the watersheds, and the shortness of the rivers (<190 km) allow rapid transport of the eroded material to the ocean (Dadson et al., 2005; Hilton, 2017; Hilton et al., 2012; Kao and Milliman, 2008; Milliman and Syvitski, 1992). Furthermore, the near absence of continental shelf along the east coast of Taiwan (Chiang and Yu, 2022) implies a direct connection of rivers to submarine canyons allowing the burial of biosphere and fossil particulate organic carbon in marine sediments through turbidity currents regardless of the variations in sea level (Hilton, 2017; Hilton et al., 2008, 2010; Kao et al., 2010, 2014).

All these mechanisms generate some of the highest sediment loads in the world, with 8 of Taiwan's 13 rivers exceeding 10,000 t km^{-2} yr^{-1},

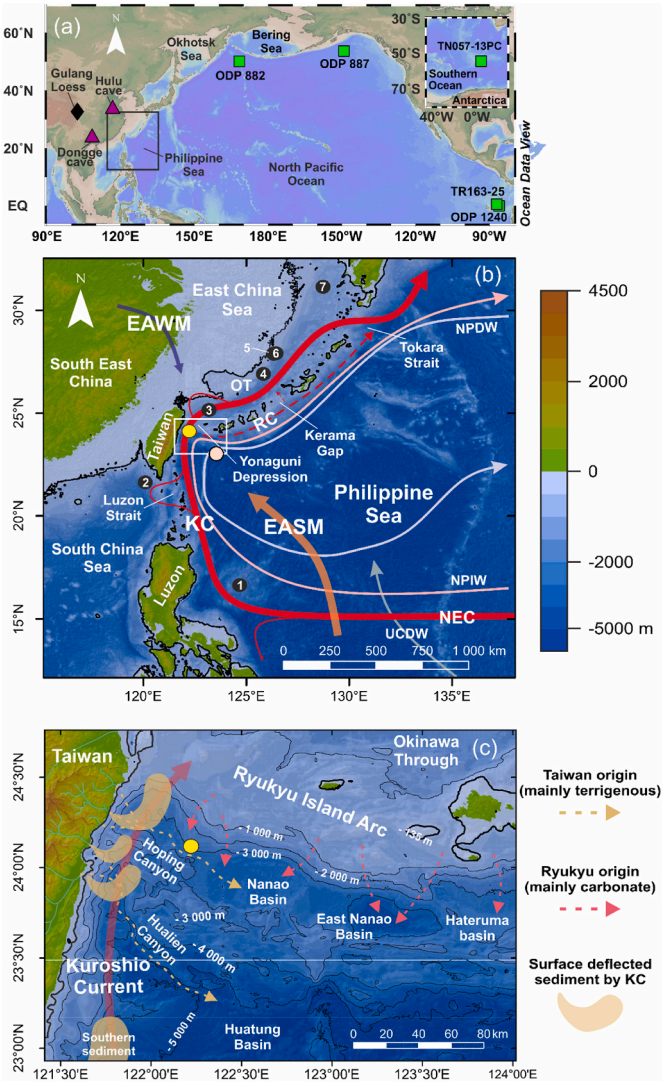

Fig. 1. Map of the study area. (a) Map of the North Pacific Ocean with an insert of the South Atlantic sector of the Southern Ocean; purple triangles: location of the Hulu and Dongge caves, black diamond: Gulang Loess record, light green rectangles: ODP sites 882 (Jaccard et al., 2009), 887 (Galbraith et al., 2007), 1240 (Jacobel et al., 2020), core TR 163-25 (Hoogakker et al., 2018) and core TN057-13 PC (Jaccard et al., 2016); black rectangle: position of the zoom of Fig. 1b. (b) Modern Kuroshio Current pathway East of Taiwan, monsoon pattern, and intermediate and deep water mass circulation (Fuhr et al., 2021) in the northwestern Philippine Sea; pink dot: location of the station in Fig. 2; white rectangle: zoom of Fib. 1c. (c) Close-up of the coring site showing bathymetry and modern sedimentary sources affecting the Hoping Canyon. Yellow dot: core MD18-3523. Black dots: cores MD06-3047 (1), MD10-3291 (2), MD01-2403 (3), MD01-2404 (4), KX12-3 (5), M063-05 (6) and CHS1 (7). NEC: North Equatorial Current, KC: Kuroshio Current, RC: Ryukyu Current, EASM: East Asian Summer Monsoon, EAWM: East Asian Winter Monsoon, OT: Okinawa Through, NPDW: North Pacific Deep Water, NPIW: North Pacific Intermediate Water, UCDW: Upper Circumpolar Deep Water. The 135 m isobath is marked by a thicker black line and shows the emerged area at the Last Glacial Maximum. (For interpretation of the references to color in this figure legend, the reader is referred to the Web version of this article.)

including three rivers from the eastern coast (Milliman and Farnsworth, 2011). Between 1970 and 1999, Taiwanese fluvial sediment discharge was 384 Mt yr^{-1} on average (Dadson et al., 2003). In northeastern Taiwan, the Hoping Canyon allows the rapid burial of sediments from the northern Central Range into the fore-arc basins of the Ryukyu wedge (Fig. 1c) (Hsiung et al., 2017; Lehu et al., 2015).

Nowadays, the east coast of Taiwan is under the influence of the Kuroshio Current, centered at 122°E and extending 85–135 km wide with a depth of 400–600 m (Jan et al., 2015). This western boundary current transports a volume of 11–23 Sv towards the north and reaches maximum current velocities between 0.7 and 1.4 m s^{-1} (Jan et al., 2015). The surface waters (0–100 m) carried by the Kuroshio Current are oligotrophic, while its subsurface (300–600 m) transports large quantities of nutrients (Chen et al., 2017; Guo, 1991). Water column

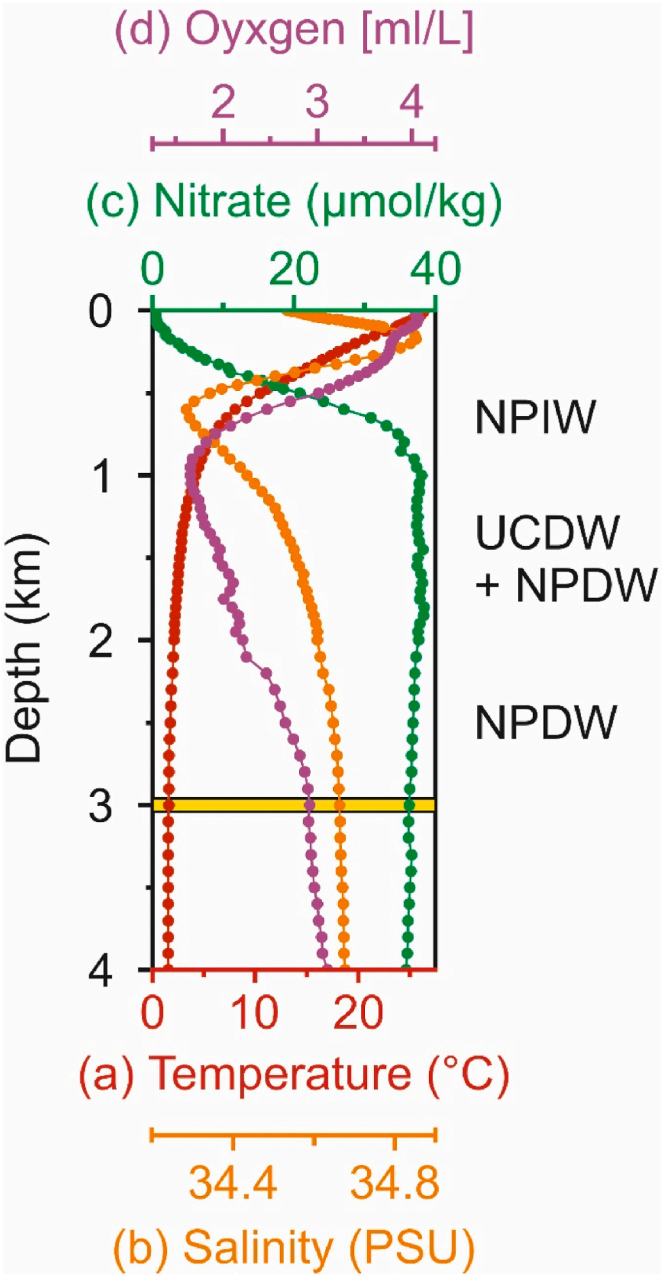

Fig. 2. Physico-chemical characteristics of water masses in the study area with (a) Temperature (°C), (b) Salinity (PSU), (c) Nitrate concentration (µmol kg^{-1}) and (d) Oxygen concentration (ml L^{-1}) versus depth (km). Data from World Ocean Atlas (2018); Garcia et al., 2019a, 2019b; Locarnini et al., 2018; Zweng et al., 2019) edited using Ocean Data View (Schlitzer, 2022). NPIW: North Pacific Intermediate Water, NPDW + UCDW: North Pacific Deep Water mixed with Upper Circumpolar Deep Water, NDPW: North Pacific Deep Water. Pink dot in Fig. 1b shows the location of the station in Fig. 2. The yellow rectangle indicates the depth of core MD18-3523. (For interpretation of the references to color in this figure legend, the reader is referred to the Web version of this article.)

salinity shows a minimum from 500 to 1000 m (Fig. 2b) characteristic of modern NPIW (You et al., 2003) associated with the beginning of an oxygen minimum. Beyond 1000 m, decreased salinity combined with high nutrients (Fig. 2c) and low oxygen concentrations (Fig. 2d) are characteristic of a mixture between oxygen-depleted UCDW (Kawabe and Fujio, 2010) and nutrient-rich North Pacific Deep Water (NPDW) (Kawabe and Fujio, 2010; Talley et al., 2011). Below 2000 m, slightly increased oxygenation (Fig. 2c) and high nutrient concentrations (Fig. 2d) indicate the presence of NPDW (Kawabe and Fujio, 2010; Talley et al., 2011).

3. Materials and methods

3.1. Core location and age model

The 21.6 m piston core MD18-3523 (24°07.40′N, 122°10.64′E; water depth 2972 m) was recovered during the EAGER Cruise aboard the R/V Marion-Dufresne II in 2018 (Babonneau and Ratzov, 2018). It was collected ~ 50 km off the east coast of Taiwan, in a levee of the Hoping Canyon (Fig. 1b). The site receives sediments from overflows of turbidity currents to the canyon originating from both Taiwan and the Ryukyu volcanic arc (Fig. 1c), and lie under the modern pathway of the Kuroshio Current (Fig. 1b). The sediment core is composed of dark grey clay with some intervening silty laminations, interpreted as terms Td and Te of the Bouma Sequence, and corresponding to overflow deposits and turbidite tails (Lehu et al., 2015). The presence of coarser silts to very fine sandy layers can be observed mainly in the first 10 m of the sediment core or between 12 and 13 m depth, possibly related to nepheloid deposits (Fenies, 2023).

The age model (Fig. 3) was built using 11 radiocarbon dates (Table 1), of which 6 were measured on *Trilobatus sacculifer* using a MICADAS-Accelerator Mass Spectrometry (AMS) at the Alfred Wegener Institute Helmholtz Centre for Polar and Marine Research (Bremerhaven, DE), and 5 on mixed planktonic foraminifera measured on the AMS at Beta Analytic (Miami, USA). Planktonic foraminifera were picked from the coarse fraction (>150 μm) of each sample. They were converted to calendar ages using Oxcal software version 4.4.4 (Ramsey, 2008) and the Marine20 calibration curve (Heaton et al., 2020). A local correction of the reservoir age of 86 ± 40 y was applied (Dezileau et al., 2016). The sedimentation rate between each radiocarbon date was calculated every 0.5 cm using Oxcal.

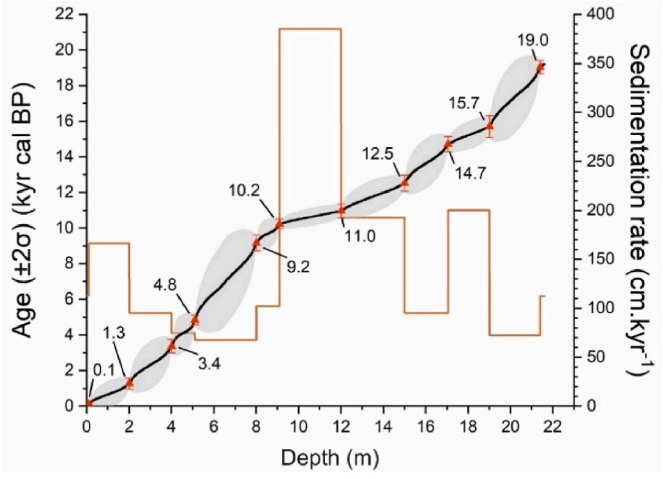

Fig. 3. Age model in kyr BP (black line) and linear sedimentation rate in cm. kyr-1 (brown line) of core MD18-3523. Red triangles indicate dated levels, with age in ka. Grey area: age model error at 2σ. (For interpretation of the references to color in this figure legend, the reader is referred to the Web version of this article.)

3.2. Reconstruction of terrestrial input, primary productivity and oxygenation changes using inorganic (XRF ratios) and organic geochemistry

The sediment core was scanned at 1 cm resolution using an ITRAX-XRF core scanner at the Department of Geoscience, National Taiwan University (Taipei, Taiwan), to determine the semi-quantitative elemental composition of the sediment in counts per second (Croudace et al., 2006).

Mn/Fe ratio was used to qualitatively reconstruct past oxygenation (Naeher et al., 2013). Br/Ti ratio was used to qualitatively reconstruct the abundance of marine organic matter and marine primary productivity (Ziegler et al., 2008). The Ti/K ratio was used as a proxy for grain size of the terrigenous fraction and intensity of physical erosion of Taiwan (Bertrand et al., 2024; Meinhold, 2010). Reasons behind the choice and use of these ratios are provided in Appendix 1 (Text S1).

Measurements of the concentration in total organic carbon (TOC) in the sediment were carried out on 216 samples spaced at ~ 10 cm, which corresponds to an average resolution of ~ 90 yr. Freeze-dried, ground and weighed samples were decarbonated by soaking ground sediment powder in 2 mol L^{-1} HCl for 4 h, then rinsed five times with Milli-Q water and centrifuged for acid removal, and dried in an oven at 50 °C overnight. They were analyzed on a Thermo Flash 2000 elemental analyzer at the Department of Oceanography, National Sun Yat-sen University (Kaohsiung, Taiwan); values are calculated using the USGS40 standard and expressed in percentage of dry weight (%). Details of the method used to differentiate between the continental and marine origin of particulate organic carbon are given in Appendix 1 (Text S2).

3.3. Planktonic foraminifera: Pulleniatina obliquiloculata abundance

The abundance of *Pulleniatina obliquiloculata* was measured on 149 of the samples used for benthic foraminiferal assemblages and reported in percentage with respect to total planktonic foraminifera counted in the >150 μm fraction. The abundance of this planktonic foraminifera was used to reconstruct the changes in the intensity of the Kuroshio Current (Baohua et al., 1997; Jian et al., 2000; Ujiié and Ujiié, 1999; Ujiié et al., 2003; Xiang et al., 2003, 2007; Xu and Oda, 1999; Xu et al., 2021; Zou et al., 2020) as this species is characteristic of Kuroshio Current waters (Lin et al., 2006).

3.4. Benthic foraminiferal assemblages

Benthic foraminifera faunal analyses were carried out on 149 samples, sampled every 20 cm between 7 – 641 cm and 1201–2160 cm (~0.2 kyr), and every 10 cm between 641 and 1201 cm (~0.1 kyr). Samples have been wet-sieved at 63 μm to separate the silt-clay fraction from the sandy fraction. Residues were dried at 40 °C, weighed and dry-sieved at 150 μm. A binocular stereomicroscope was used to count around 300 specimens of benthic foraminifera per sample, or as many as present, from the >150 μm fraction. When benthic foraminifera numbers were expected to be substantially higher than 300, the samples were split using a micro-splitter. Species abundance is given as a percentage with respect to all benthic foraminifera counted in the >150 μm fraction. Benthic foraminifera were identified to species or genus level following the classification of Loeblich Jr and Tappan (1988) and the taxonomical descriptions of several authors (Boltovskoy et al., 1980; Cage et al., 2021; Cushman, 1933; Hanagata and Nobuhara, 2015; Holbourn et al., 2013; Holbourn and Henderson, 2002; Lei and Li, 2016; Symphonia and Senthil, 2019; Wilson, 2013). The original taxonomy has been standardized using the taxonomy validated to date of the World Register of Marine Species foraminifera database (Hayward et al., 2020). A selection criterion to establish which species were representative of the overall benthic foraminifera population observed was fixed at abundance of 5% in at least 2 samples, enabling the identification of 31 benthic foraminifera taxa representing on average 91.2% (±15.1)

Table 1
AMS^{14}C ages and instrumental error (y), calendar ages and error in ka (±2σ) on the sediment core MD18-3523.

Lab ID	Material	Depth (cm)	AMS^{14}C age (yr cal)	Error (yr cal)	Calibrated Age (ka)	Standard Error (ka, ±2σ)
Beta - 564432	Mixed planktonic foraminifera	10.5	720	30	0.1	0.2
7619	*Trilobatus sacculifer*	201.0	1939	79	1.3	0.3
7620	*Trilobatus sacculifer*	401.0	3708	85	3.4	0.4
Beta - 559540	Mixed planktonic foraminifera	510.5	4860	30	4.8	0.3
7621	*Trilobatus sacculifer*	801.0	8771	111	9.2	0.5
Beta - 559541	Mixed planktonic foraminifera	910.5	9640	30	10.2	0.3
7622	*Trilobatus sacculifer*	1201.0	10122	97	11.0	0.4
7623	*Trilobatus sacculifer*	1501.0	11262	127	12.5	0.5
Beta - 559542	Mixed planktonic foraminifera	1705.5	13090	40	14.7	0.4
7624	*Trilobatus sacculifer*	1901.0	13716	155	15.7	0.6
Beta - 564433	Mixed planktonic foraminifera	2140.5	16600	50	19.0	0.4

(±2σ; as all the confidence interval given hereafter throughout the manuscript) of all benthic foraminifera found in each sample (Appendix 2; Table S1).

3.5. Multivariate analysis and statistical tests

As benthic foraminifera assemblages respond rapidly to changes in physico-chemical conditions, multivariate analyses are commonly used to study their evolution, with the aim of summarizing the variations in taxa observed throughout the record. These methods can be used to identify and visualize patterns, synthesize the control exerted by environmental parameters on the benthic foraminiferal community and ultimately reconstruct past environmental changes based on the ecology of benthic foraminifera (e.g. Angue Minto'o et al., 2015; Belanger et al., 2020; Courtillat et al., 2020; Hayward et al., 2001; Sharon and Belanger, 2022; Tetard et al., 2017). In deep marine environments, the main environmental parameters that influence the distribution of benthic foraminifera are oxygenation and the availability/quality of food (Gooday, 2003; Gooday and Jorissen, 2012; Jorissen et al., 2007) as conceptualized by the TROX (TRophic conditions and OXygen concentrations) model (Jorissen et al., 1995; Levin and Gage, 1998; Van der Zwaan et al., 1999). In this study, the core has been collected on the Hoping canyon levee, and consequently, is also influenced by the turbidity currents generated by Taiwan's physical erosion. It is especially the case during extreme events such as typhoons or earthquakes (Dadson et al., 2005; Lehu et al., 2015, 2016) that may cause post-mortem downslope transport of benthic foraminifera and inputs of terrestrial organic matter. Multivariate analyses were carried out on the 31 benthic foraminiferal taxa showing an abundance greater than 5% in at least 2 samples (Appendix 2; Table S2). Prior to any multivariate analysis, *Quinqueloculina* spp. and *Triloculina* spp. were grouped together as "shelf miliolids", as they come from the same water depth (inner shelf to shelf zone, Murray, 2006; Polonia et al., 2023) and share a similar ecology (Murray, 2006).

3.5.1. Hierarchical cluster analysis (HCA)

The R-mode HCA was performed using Ward's method, which agglomerates taxa by minimizing the within-clusters sum of squares (Ward, 1963). Details of the method used to perform the HCA can be found in Appendix 1 (Text S3.1). Prior to the HCA, the relative abundance of the taxa underwent an arcsine of the commonly used square root transformation (Chan et al., 2022; Duros et al., 2011; Fanget et al., 2016; Fontanier et al., 2008, 2015; Goineau et al., 2011; Gooday et al., 2010; Haller et al., 2018; Nunes et al., 2023) in order to stabilize the variance and reduce the influence of extreme values (Parker and Arnold, 1999; Sen Gupta, 1999). The HCA enabled to group the taxa sharing similar temporal distributions throughout the core into biofacies. To visualize the evolution of these biofacies over the last 20,000 years, for each sample, the relative abundances of each of the taxa included in each biofacies was summed to obtain a relative abundance for each biofacies that indirectly represents the extent to which the palaeoenvironmental conditions that enabled these species to develop are in place (Angue Minto'o et al., 2015; Courtillat et al., 2020). This approach allow us to reconstruct changes in the paleoenvironment independently of geochemical measurements.

3.5.2. Detrended correspondence analysis (DCA) and distance-based redundancy analysis (db-RDA)

The body of literature concerning the ecology of taxa and benthic foraminiferal responses to variables like oxygen, food quality/quantity, and continental erosion is relatively scarce and at times contradictory. For example, foraminifera that thrive on high organic matter also prefer low-oxygen environments, and organic matter can come from both marine productivity and continental erosion. To clarify the influence of each environmental parameter, a constrained ordination analysis was performed to better understand the influence of environmental (constraining) variables on the benthic foraminiferal community and improve past environmental reconstructions from biofacies.

To determine whether the ordination method employed should be linear or unimodal, we performed a DCA (Hill and Gauch, 1980) to obtain the length of axis 1 (Fig. S1). Details of the method used to perform the DCA can be found in Appendix 1 (Text S3.2) and details of DCA results can be found in Appendix 3. As the length was 3.1, in the grey zone between length <3 (= linear method) and >4 (= unimodal method), both methods can be used (Lepš and Šmilauer, 2003). Therefore, a db-RDA was performed (Legendre and Anderson, 1999). Details of the method used to perform the db-RDA can be found in Appendix 1 (Text S3.2). This linear method is similar to classic Redundancy Analysis (RDA), but allows the use of a Bray-Curtis distance matrix, which is better suited to the study of species abundance data than Euclidian distance classically used in RDA (Legendre and Anderson, 1999; Ricotta and Pavoine, 2022).

3.5.3. Correlation coefficient matrices

A Spearman correlation matrix was generated between the bottom – pore water transfer functions (EBFOI, BFA), the Mn/Fe bulk ratio, the biofacies B and C abundance and the *P. obliquiloculata* abundance to observe the relationships between them. Only samples containing all the variables to be correlated were included. Samples with one or more missing variables were excluded before correlation analysis.

3.6. Quantitative reconstructions of bottom – pore water oxygenation

Bottom – pore water oxygenation was quantitatively reconstructed using two equations: the Benthic Foraminifera Assemblage (BFA) index from Tetard et al. (2021) and the Enhanced Benthic Foraminifera Oxygen Index (EBFOI) from Kranner et al. (2022). The details behind the choice of transfer functions used are available in Appendix 1 (Text S4). Transfer functions were applied on two subsets of data, the first one contains the 31 benthic foraminiferal taxa showing an abundance greater than 5% in at least 2 samples (BFA_{31} and $EBFOI_{31}$) and the second one only 27 of these 31 taxa after removing those whose presence

at the water depth of the coring site is not expected, and are therefore potentially transported (BFA_{27} and $EBFOI_{27}$).

The terminology to describe oxygen levels in water masses follows Kaiho (1994): "oxic" (>1.5 ml L^{-1}), "suboxic" (1.5–0.3 ml L^{-1}), "dysoxic" (0.3–0.1 ml L^{-1}) and "anoxic" (0.1–0.0 ml L^{-1}) waters. The assignment of oxygenation categories to taxa is based on previous studies, with preferences given to the studies based on modern observations (Appendix 2; Table S2).

3.7. Semi-quantitative reconstruction of benthic foraminifera productivity

The Benthic Foraminifera Accumulation Rate (BFAR) was used as a semi-quantitative proxy for organic matter flux to the sea floor and benthic foraminifera productivity (Herguera, 1992, 2000; Herguera and Berger, 1991; Jorissen et al., 2007). The BFAR (ind g^{-1} cm^{-2} kyr^{-1}) was calculated by multiplying the number of benthic foraminifera per gram of total dry sediment (NbBF; ind g^{-1}) by the linear sedimentation rate (LSR; cm kyr^{-1}) and the dry bulk density (D_{dry}; g cm^{-3}) (Herguera, 2000). Details of the equation used are provided in Appendix 1 (Text S5).

4. Results

4.1. Age model and sedimentation rate

The age model indicates that the sediment core MD18-3523 ranges from 19 to 0.090 ka (±0.173 ka), covering the transition from Marine Isotope Stage (MIS) 2 (27.8–14.7 ka) to MIS 1 (14.7–0 ka) (Sanchez Goñi and Harrison, 2010), from the end of the LGM to the Holocene (11.7–0.0 ka; Walker et al., 2012). It shows an average linear sedimentation rate of ~ 157 cm kyr^{-1} (Fig. 3). Three periods of higher sedimentation rate are observed: (i) 166 cm kyr^{-1} from 1.3 to 0.1 ka, (ii) 287 cm kyr^{-1} from 12.5 to 10.2 ka, from the Younger Dryas (YD; 12.9–11.7; Clark et al., 2012) to the beginning of the Early Holocene (11.7–8.2 ka; Walker et al., 2012), and (iii) 200 cm kyr^{-1} from 15.7 to 14.7 ka, during the late HS1. A maximum of 385 cm kyr^{-1} is reached during the Early Holocene between 10.2 ka and 11.0 ka (Fig. 3).

4.2. Benthic foraminifera assemblages and multivariate analysis

In total, we identified 151 taxa of benthic foraminifera including 31 taxa with an abundance of over 5% in at least two samples (Appendix 2; Table S2), representing on average 91.2% (±15.1) of all benthic foraminifera present in each sample.

4.2.1. Results of the multivariate analysis

The R-mode hierarchical cluster analysis show a cophenetic correlation of 0.81 between the original dissimilarity matrix and the cophenetic matrix. It allows us to identify 3 benthic foraminifera biofacies (Fig. 4).

The results of the db-RDA show that the constraining variables explain 17.49% of the total variance in the benthic foraminiferal community (see Appendix 3 for details of the db-RDA results). The inflation factor variances of all the constraining variables are smaller than 5. The ANOVA performed on the results of the db-RDA shows that the db-RDA itself and each of its variables are significant (p-value <0.001), demonstrating that the constraining variables chosen are relevant to explain the variations observed in the benthic foraminiferal population. The ANOVA performed on the axis shows that only the first two axes of the db-RDA significantly explain the variation in benthic foraminifera taxa by the constraining environmental variables (p-value <0.001). The db-RDA results show that the two first axis explain 95.65% of the constrained proportion of the variance, with axis 1 and axis 2 explaining respectively 64.94% and 30.71% of this variance. On the db-RDA correlation triplot (Fig. 5), the axis 1 is distinguished by a negative correlation with Br/Ti (r = - 0.70) and positive correlation with Mn/Fe (r = 0.51) and Ti/K (r = 0.12), while axis 2 is characterized by a negative correlation with Ti/K (r = −0.60) and a positive correlation with Mn/Fe (r = 0.24) and Br/Ti (r = 0.14). The correlations between benthic foraminiferal taxa and environmental variables are positive when the taxa are projected in the same direction as the environmental arrows, and negative when they are projected in the opposite direction. For the environmental variables themselves, correlations are positive when environmental arrows form an acute angle, negative when they form an obtuse angle and null when they form a right angle (Fig. 5).

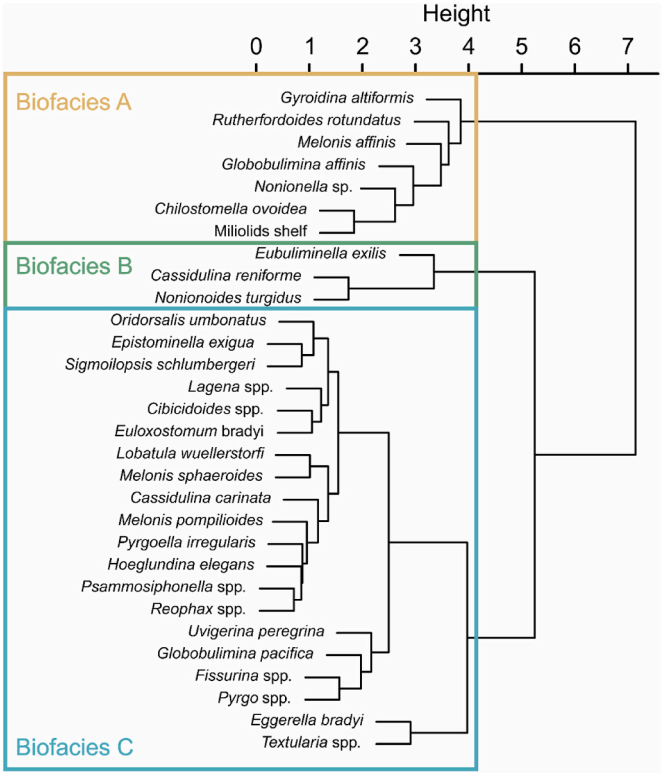

Fig. 4. Hierarchical cluster analysis (HCA) of benthic foraminifera taxa showing an abundance higher than 5% in at least two samples.

4.2.2. Summary of the composition and ecology of biofacies

Biofacies A is composed of suboxic to dysoxic infaunal taxa (*C. ovoidea*, *G. affinis*, *R. rotundatus* and *M. affinis*) that appreciate high fluxes of organic matter, potentially terrestrial and deposited by turbidity currents (Bernhard et al., 1997; Cannariato et al., 1999; Caralp, 1989; De and Gupta, 2010; Fontanier et al., 2003; Glock, 2023; Hess et al., 2005; Koho et al., 2008; Mojtahid et al., 2009; Nomaki et al., 2006; Rathburn et al., 1996; Rathburn and Corliss, 1994; Schmiedl et al., 1997, 2000, 2000, 2000; Schonfeld, 2001; Zarriess and Mackensen, 2010), and of taxa transported post-mortem from bathymetric zones higher up the slope (*G. altiformis*, *Quinqueloculina* spp., *Triloculina* spp., *Nonionella* sp.) (Barbieri, 1991; Culver, 1988; Duchemin et al., 2007; Fiorini, 2015; McGann et al., 2003; Murray, 2006; Polonia et al., 2023; Smith et al., 2001; Smith and Gallagher, 2003).

Biofacies B is composed of dysoxic infaunal taxa preferring fresh/labile marine organic matter from phytoplankton (Caralp, 1989; Caulle et al., 2014; Goineau et al., 2011, 2015; Ohkushi et al., 2018; Zarriess and Mackensen, 2010) and does not present any taxa which may come from a bathymetric zone higher up the slope.

Biofacies C is composed of 69.00% oxic taxa, 17.01% of suboxic taxa and 13.32% of dysoxic taxa. Suboxic to oxic opportunistic taxa that thrive on seasonal or sporadic inputs of fresh organic matter (*Cibicidoides* spp., *H. elegans*, *L. wuellerstorfi*, *Pyrgo* spp., *P. irregularis*, *O. umbonatus*, *E. exigua*, *Psammosiphonella* spp., *M. pompilioides*, *M. sphaeroides*, *E. bradyi*,

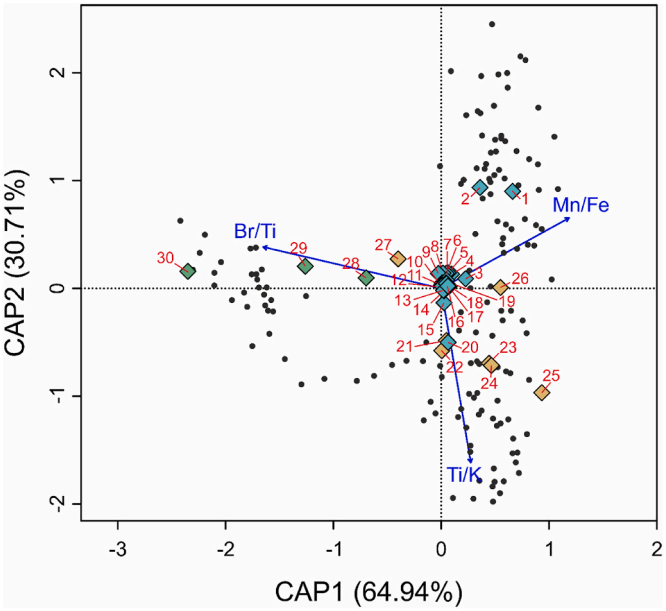

Fig. 5. Distance-based redundancy analysis (db-RDA) scaling 2/correlation triplot showing the relationship between benthic foraminiferal taxa and the environmental variables (in dark blue): Mn/Fe as indicative of the bottom – pore water dissolved oxygen concentration, Br/Ti for the organic matter derived from the marine primary productivity and Ti/K for the erosion of Taiwan and the hydro-sedimentary activity associated. The number indicate benthic foraminiferal taxa. The taxa of the biofacies C are colored in light blue: 1. Eggerella bradyi, 2. Textularia spp., 3. Globobulimina pacifica, 4. Euloxostomum bradyi, 5. Oridorsalis umbonatus, 6. Epistominella exigua, 7. Lagena spp., 8. Melonis sphaeroides, 9. Lobatula wuellerstorfi, 10. Reophax spp., 11. Psammosiphonella spp., 12. Pyrgoella irregularis, 13. Hoeglundina elegans, 14. Cassidulina carinata, 15. Pyrgo spp., 16. Cibicidoides spp., 17. Sigmoilopsis schlumbergeri, 18. Fissurina spp., 19. Melonis pompilioides, 20. Uvigerina peregrina. The taxa of the biofacies A are colored in brown: 21. Chilostomella ovoidea, 22. Shelf miliolids, 23. Nonionella sp., 24. Rutherfordoides rotundatus, 25. Gyroidina altiformis, 26. Globobulimina affinis, 27. Melonis affinis. The taxa of the biofacies B are colored in forest green: 28. Nonionoides turgidus, 29. Cassidulina reniforme, 30. Eubuliminella exilis. (For interpretation of the references to color in this figure legend, the reader is referred to the Web version of this article.)

Textularia spp. and *S. schlumbergeri*) represent on average 52.54% of the taxa in biofacies C (Altenbach et al., 1999; Caulle et al., 2014; Chauhan et al., 2016; De and Gupta, 2010; Dessandier et al., 2015; Enge et al., 2012; Geslin et al., 2004; Gooday, 1988; Jorissen and Wittling, 1999; Kitazato et al., 2000; Kuhnt et al., 1996; Langlet et al., 2014; Linke and Lutze, 1993; Lutze and Thiel, 1989; Mackensen et al., 1995; Murgese and De Deckker, 2005; Ohga and Kitazato, 1997; Ohkushi et al., 2013; Rathburn et al., 1996; Rathburn and Corliss, 1994; Schmiedl et al., 1997; Schonfeld, 2001; Sousa et al., 2006; Vicente et al., 2021; Zarriess and Mackensen, 2010). Other suboxic species (*U. peregrina* and *C. carinata;* 14.28% of the taxa in biofacies C) may be pioneers in the recolonization of environments affected by the influx of organic matter through turbidity currents (Cannariato et al., 1999; De Rijk et al., 2000; Duchemin et al., 2007; Hess et al., 2005; Mackensen et al., 1995; Palmer et al., 2020; Rathburn and Corliss, 1994; Schmiedl et al., 1997; Uchimura et al., 2017; Zarriess and Mackensen, 2010). Other oxic taxa within this biofacies have an unclear ecology, either ecto-parasites or suspension feeders (*Fissurina* spp. and *Lagena* spp.; 18.74% of the taxa in biofacies C) (Collen and Newell, 1999; Haynes, 1981; Kurtarkar et al., 2024; Ranju et al., 2022; Rathburn and Corliss, 1994) or species that may appreciate strong inputs of organic matter (*Reophax* spp.; 0.45% of the taxa in biofacies C) (Enge et al., 2012; Fontanier et al., 2005; Ohkushi and Natori, 2001; Schonfeld, 2001; Sousa et al., 2024; Szarek et al., 2007; Vicente et al., 2021; Yamashita et al., 2019). The two main dysoxic deep infaunal species (13.32% of the taxa in biofacies C) are favoured by high organic matter concentration in sediments (*Eu. bradyi* and *G. pacifica*) and are also commonly found under suboxic bottom water conditions (Das et al., 2017; Mazumder and Nigam, 2014). Biofacies C does not contain any taxa which may come from a bathymetric zone higher up the slope.

Detailed description of the ecology of all species based on the scientific literature and the results of the db-RDA are available in Appendix 1 (Text S6).

4.3. Correlation matrices between proxies related to bottom – pore water oxygenation

The values of the transfer functions $EBFOI_{31}$, BFA_{31}, $EBFOI_{27}$ and BFA_{27} show strong to very strong Spearman correlation coefficients with each other, as well as strong to moderate correlations with the abundance of biofacies B and C (Table 2). The log(Mn/Fe) values show moderate Spearman correlation coefficients with the bottom – pore water oxygenation transfer functions and the biofacies B and C (Table 2). The *P. obliquiloculata* abundance show moderate correlation coefficients with the bottom – pore water oxygenation values reconstructed by the transfer functions, the log(Mn/Fe) values and the biofacies B and C abundance (Table 2).

4.4. Temporal evolution of the biofacies, BFAR, bottom – pore water oxygenation and geochemical proxies throughout the record

The Br/Ti ratio, the BFAR, the TOC concentration and the abundance of the biofacies C indicate an enhanced marine primary productivity and flux of labile organic matter to the sea floor from the end of the Last Glacial Maximum to the end of HS1, followed by a gradual decline during the BA until reaching a minimum during the YD and remaining weak thereafter (Fig. 6b, f, 6h and 6j).

The Mn/Fe ratio indicates reduced oxygenation of bottom waters from the end of the LGM to the end of the HS1, then an increase until the Middle Holocene marked by a period of stagnation from the middle of the BA to the middle of the Early Holocene (Fig. 6e). During the Middle and Late Holocene, the Mn/Fe ratio suggests that oxygenation conditions remain stable (Fig. 6e). The increase in bottom – pore water oxygenation during the last glacial-interglacial transition is also evidenced by the benthic foraminiferal assemblages and EBFOI and BFA transfer functions (Fig. 6b to d). Biofacies B, composed solely of dysoxic taxa, show high abundance from the end of the LGM to the end of HS1, then a decline during the BA and almost disappearance after that (Fig. 6b). Biofacies C, composed mainly of oxic and suboxic taxa, is almost absent from the end of the LGM until the end of HS1, and begins to increase during the BA before marking a halt from the middle of the BA until the middle of the Early Holocene, then resuming its increase until the Middle Holocene and remaining stable until the middle of the Late Holocene (Fig. 6b). The last 2 ka of the Late Holocene are marked by a significant drop in the abundance of biofacies C from 2 to 1 ka, followed by an increase (Fig. 6b). The dissolved oxygen concentration of bottom – pore waters reconstructed from transfer functions shows a similar pattern and, depending on the choice of transfer function (EBFOI and BFA), a transition from suboxic or anoxic conditions from the end of the LGM to the end of HS1 towards oxic or suboxic conditions during the Holocene (Fig. 6c and d).

The Ti/K ratio and the abundance of the biofacies A, containing numerous taxa transported post-mortem, indicate a reduced transport of terrestrial material from Taiwan and diminished hydro-sedimentary activity in the Hoping Canyon from the end of the LGM to the end of HS1 (Fig. 6a and g). From the BA to the Early Holocene and during the last 2 kyr of the Late Holocene, these proxies in conjunction with the TOC concentration and the BFAR, indicate an increased transport of terrigenous material from Taiwan to the sea floor, including terrestrial

Table 2
Spearman correlation matrix between the bottom – pore water reconstructions obtained using the transfer functions Enhanced Benthic Foraminifera Oxygen Index (EBFOI) and the Benthic Foraminifera Assemblages (BFA) index, the abundance of biofacies B and C and the log(Mn/Fe) with the abundance of the planktonic foraminifera Pulleniatina obliquiloculata. The transfer functions have been applied to the 31 taxa with an abundance greater than 5% in at least two samples ($EBFOI_{31}$ and BFA_{31}), and to 27 of these 31 taxa by removing taxa from a different bathymetric region ($EBFOI_{27}$ and BFA_{27}). Values in bold show a p-value significantly <0.001.

Variables	$EBFOI_{31}$	BFA_{31}	$EBFOI_{27}$	BFA_{27}	Biofacies B abundance	Biofacies C abundance	Log(Mn/Fe)	*Pulleniatina obliquiloculata* abundance
$EBFOI_{31}$	**1**	**0.98**	**0.93**	**0.80**	**−0.51**	**0.84**	**0.58**	**0.48**
BFA_{31}		**1**	**0.93**	**0.81**	**−0.55**	**0.84**	**0.61**	**0.48**
$EBFOI_{27}$			**1**	**0.84**	**−0.60**	**0.87**	**0.62**	**0.51**
BFA_{27}				**1**	**−0.57**	**0.63**	**0.53**	**0.47**
Biofacies B abundance					**1**	**−0.64**	**−0.56**	**−0.61**
Biofacies C abundance						**1**	**0.62**	**0.56**
Log(Mn/Fe)							**1**	**0.47**
Pulleniatina obliquiloculata abundance								**1**

organic matter, and enhanced hydro-sedimentary activity in the Hoping Canyon (Fig. 6a, g, 6h and 6j).

The changes in the relative abundance of *P. obliquiloculata* indicate a weakened Kuroshio Current from the end of the LGM to the end of the HS1, followed by an intensification until reaching a maximum during the Middle Holocene (Fig. 6i). The collapse in the abundance from 5 to 3 ka (Fig. 6i) is comparable to that observed in other cores along the path of the Kuroshio Current during this interval and is known as the *Pulleniatina* Minimum Event (Lin et al., 2006). The reasons behind this phenomenon remain unclear and may not be related to a decrease in the intensity of the Kuroshio Current (Lin et al., 2006). However, the overall decline from the Middle Holocene to the Late Holocene suggests a weakening of the Kuroshio Current over this period (Fig. 6h).

5. Discussion

Despite slight differences in the trends and in absolute values, $EBFOI_{31}$ and $EBFOI_{27}$, and BFA_{31} and BFA_{27} reconstruct similar bottom – pore water oxygenation conditions and a common trend throughout the records as evidenced by the strong to very strong Spearman correlation coefficients ($r = 0.80$ to 0.98) (Table 2). It can therefore be concluded that the contamination of the assemblages by the post-mortem transport of taxa from bathymetric zones situated at a greater depth to the study site does not appear to have significantly affected the reconstruction of bottom water oxygenation. This reinforces confidence in the reconstruction, despite the complicated sedimentological context.

The benthic foraminiferal composition of biofacies A indicates that the environment was significantly influenced by the canyon's hydro-sedimentary activity, transporting post-mortem taxa tests from higher up the slope, and bringing a substantial quantity of continental material from Taiwan's erosion, particularly continental organic matter. Upon reaching the sea floor, the part of the organic matter that escapes degradation in the water column will be subject to the effects of oxidation at the surface and inside the sediments, resulting in the development of dysoxic to suboxic bottom – pore water conditions. Biofacies B indicates an environment subject to high fluxes of labile marine organic matter in a context of intense marine primary productivity and low bottom – pore water oxygenation, which may be caused or enhanced by organic matter degradation. Biofacies C indicates an average oxic to suboxic bottom – pore water oxygenation, coupled with low primary productivity and an overall reduction in the flux of organic matter to the sea floor and in the canyon hydro-sedimentary activity. However, the faunal composition also shows that the environment reconstructed can be occasionally subject to influxes of organic matter from turbidity currents. Both biofacies B and C appear to be unaffected by the post-mortem transport of shallower taxa.

5.1. Changes in the marine biological pump efficiency since the end of the last glacial maximum and impact on the carbon storage during the HS1

The increase in the oxygenation of intermediate water masses in the North Pacific above 2000 m during HS1 is relatively well established (e.g. Chang et al., 2014; Ohkushi et al., 2013; Okazaki et al., 2010; Shibahara et al., 2007; Zou et al., 2020), however the water depth influenced by this increased oxygenation is not well constrained. Previous studies infer higher oxygenation than during the LGM down to 3000 m in the North Pacific (Duplessy et al., 1988; Okazaki et al., 2010; Rae et al., 2014) while others suggest that the increase in oxygenation is confined above 2000 m (Gong et al., 2019; Jaccard and Galbraith, 2013; Keigwin, 1998; Lu et al., 2020; Matsumoto et al., 2002; Rae et al., 2020).

The three methods applied here to reconstruct past oxygenation changes since the end of the LGM (HCA, transfer functions based on benthic foraminiferal assemblages and sedimentary elemental ratios) indicate suboxic-dysoxic (maybe even anoxic) conditions during the HS1, followed by an increase of bottom – pore water oxygenation at the BA to reach oxic-suboxic conditions during the Holocene (Fig. 7c to f). The coherence among the proxies is verified by the moderate to very strong degree of Spearman correlations between $EBFOI_{31}$, $EBFOI_{27}$, BFA_{31}, BFA_{27}, Biofacies B, Biofacies C and Mn/Fe ($|r| = 0.51$–0.98) (Table 2). In average, the Mn/Fe ratio shows the lowest degree of correlation with others proxies, emphasized by the absence of decline in pore – water oxygenation from 2 to 1 ka, whereas the other oxygenation proxies all exhibit it (Fig. 7c to f). This might be attributed to a lower sensitivity of chemical elements in marine sediments to changes in oxygenation compared to benthic foraminifera.

Thus, all the bottom – pore water paleoxygenation proxies support the hypothesis of an enhanced oxygenation confined to the first 2000 m of the water column during the HS1 despite the intensification of the PMOC due to an increase in glacial NPIW formation by saltier Bering and Okhotsk Sea (Fig. 1a) (Ohkushi et al., 2003; Okazaki et al., 2010, 2012; Rae et al., 2020). This lack of penetration of the dense waters to the deep ocean might be explained by the occurrence of a stratification front between NPIW and NPDW due to the salinity increase of the glacial NPIW during HS1 (Gong et al., 2019; Rae et al., 2020).

This result is consistent with the paleo-circulation reconstructions derived from authigenic uranium concentration at ODP Sites 882 and 887, located at 3244 m in the northwest (Jaccard et al., 2009) and 3647 m in the northeast North Pacific (Galbraith et al., 2007), from benthic foraminiferal gradient $\Delta\delta^{13}C$ in core TR163-25 located at 2650 m in the eastern equatorial North Pacific (Hoogakker et al., 2018), and authigenic uranium at ODP Site 1240 located at 2921 m in the eastern equatorial North Pacific (Jacobel et al., 2020) (Figs. 7g and 1a). The synchronous bottom oxygenation rise during the BA at our study site (Fig. 7e and f) with those observed in the ODP sites 882 and 1240, and core TR163-25 (Fig. 7g) suggests that changes in the bottom – pore water oxygenation pattern in the northwestern Philippine Sea are at

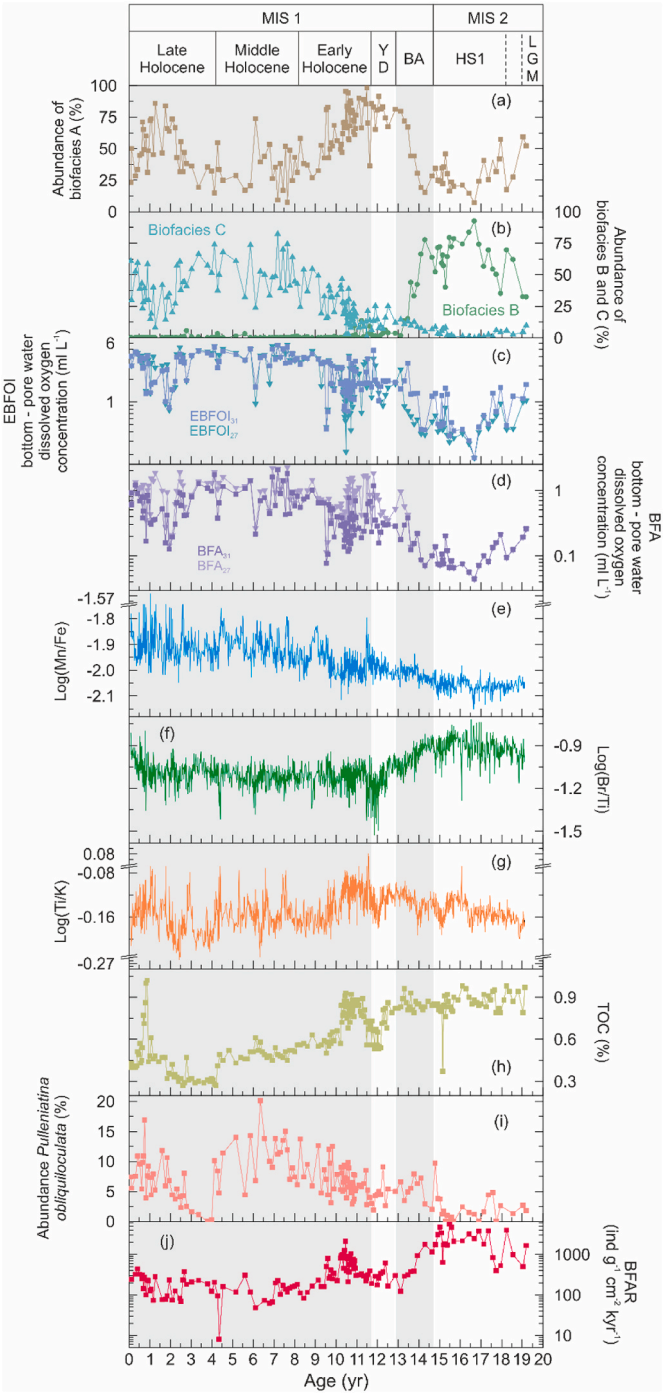

Fig. 6. Results on core MD18-3523: (a) Abundance of biofacies A (%), (b) Abundance of biofacies B (green dot) and C (light blue triangle), (c to d) bottom – pore water dissolved oxygen concentration reconstructed using (c) the Enhanced Benthic Foraminifera Oxygen Index (EBFOI; Kranner et al., 2022) and (d) the Benthic Foraminiferal Assemblage (BFA; Tetard et al., 2021), both transfer functions have been applied to the 31 taxa with an abundance greater than 5% in at least two samples ($EBFOI_{31}$ and BFA_{31}; dots), and to 27 of these 31 taxa by removing taxa from a different bathymetric region ($EBFOI_{27}$ and BFA_{27}; inverted triangles); (e) log(Mn/Fe), (f) log(Br/Ti), (g) log(Ti/K), (h) Total Organic Carbon (TOC; %), (i) abundance of Pulleniatina obliquiloculata (%) and (j) Benthic Foraminifera Accumulation Rate (BFAR; ind. g^{-1} cm^{-2} kyr^{-1}). The marine isotope stages (MIS) are subdivided into millennial-scale periods with: Last Glacial Maximum (LGM), Heinrich Stadial 1 (HS1), Bølling-Allerød (BA), Younger Dryas (YD). Grey areas indicate warm periods. (For interpretation of the references to color in this figure legend, the reader is referred to the Web version of this article.)

least partly related to basin-wide mechanism. At a global scale, the low oxygenation of the deep water masses (>2000 m depth) during HS1 can be mainly attributed to the persistence of a sluggish ventilation inherited from the LGM (Menviel et al., 2017, 2020; Sigman et al., 2021; Skinner et al., 2010; Wu et al., 2018) and the delay in propagation of oxygenated water masses from the Southern Ocean to the North Pacific (more than 2 kyr during HS1) (de la Fuente et al., 2015) originating from the intensification of the AABW formation during HS1 (Anderson et al., 2009; Jaccard et al., 2016; Wang et al., 2024; Wu et al., 2018). After HS1, the oxygenated abyssal water masses begin to arrive in the North Pacific and the oxygenation increases. Then, the second intensification of formation of AABW during the YD (Fig. 7h) allows the concentration in dissolved oxygen of deep water masses to reach that of the Holocene.

These changes in the AABW formation intensity at the beginning of the deglaciation can be attributed to the poleward migration of the Southern Hemisphere Westerlies resulting in an increase in the northward Ekman transport of surface waters and enhancement of the Southern Ocean upwelling, as evidenced by the increase in opal production (Fig. 7h) in core TN057-13 PC located in the Atlantic part of the Southern Ocean (Fig. 1a), due to an intense cooling in the Northern Hemisphere generated by the collapse of the Atlantic Meridional Oceanic Circulation (AMOC) (Anderson et al., 2009; Denton et al., 2010; McManus et al., 2004a) (Fig. 7i). It would have also reduced the residence time of the surface water masses in the Antarctic Zone, weakening the halocline and strengthening the AABW formation (Sigman et al., 2021). These mechanisms might have been combined with other mechanisms. The increase of the sea level (Fig. 7j) might have caused the decline of the sea ice equatorward expansion, resulting in the reduction of the brine export to the ocean interior and therefore a reduction in stratification by lowering the salinity of the upper water masses (Bouttes et al., 2010; Sigman et al., 2021). This decline of the sea ice expansion might also have led to the retreat of the buoyancy loss region, resulting in an even greater reduction of the residence time of the surface water masses in the Antarctic Zone and weakening even more the halocline (Sigman et al., 2021; Watson et al., 2015). Another mechanism might have been the deepening of the abyssal mixing causing the increase in the AABW formation (Lynch-Stieglitz et al., 2007; Sigman et al., 2021). Finally, the warming of the water column might have led to another reduction of the surface water masses residence time by weakening the importance of the salinity in the density stratification of the upper ocean (de Boer et al., 2007; Sigman et al., 2004).

Global mechanisms can be complemented by regional ones, as observed in the influence of volcanic eruptions during the deglaciation on bottom water oxygenation at the ODP 1418 site, which is located at depth of 3680 m in the Gulf of Alaska (Du et al., 2022). One of them is the intensification of the Kuroshio Current after HS1 as evidenced by the increase in the relative abundance of the planktonic foraminifera *P. obliquiloculata* (Fig. 7b). This species is believed to be a bio-indicator of the Kuroshio Current intensity current (Baohua et al., 1997; Jian et al., 2000; Ujiié and Ujiié, 1999; Ujiié et al., 2003). The moderate degree of Spearman correlation ($|r| = 0.47–0.61$) observed between the relative abundance of *P. obliquiloculata* and the bottom – pore water oxygenation proxies (Table 2), as well as the similarity of the trends observed (Fig. 7) suggest a potential link between Kuroshio Current intensity and bottom – pore water oxygenation.

During HS1, the cooling of the Northern Hemisphere by the occurrence of the perihelion during the boreal spring (Clement et al., 1999) and the slowdown of the AMOC (Fig. 7i) due to the iceberg discharge in the North Atlantic (Lynch-Stieglitz, 2017; McManus et al., 2004b) led to the southward migration of the Intertropical Convergence Zone (ITCZ) (Stager et al., 2011), resulting in the weakening of the equatorial trade winds and the establishment of an El Niño-like state in the equatorial Pacific (Clement et al., 1999; Yang et al., 2023). This atmospheric configuration is characterized by a weaker Walker circulation (Yu et al., 2023) which, combined with a weaker EASM (Cheng et al., 2016), would have resulted in a northward migration of the North Equatorial

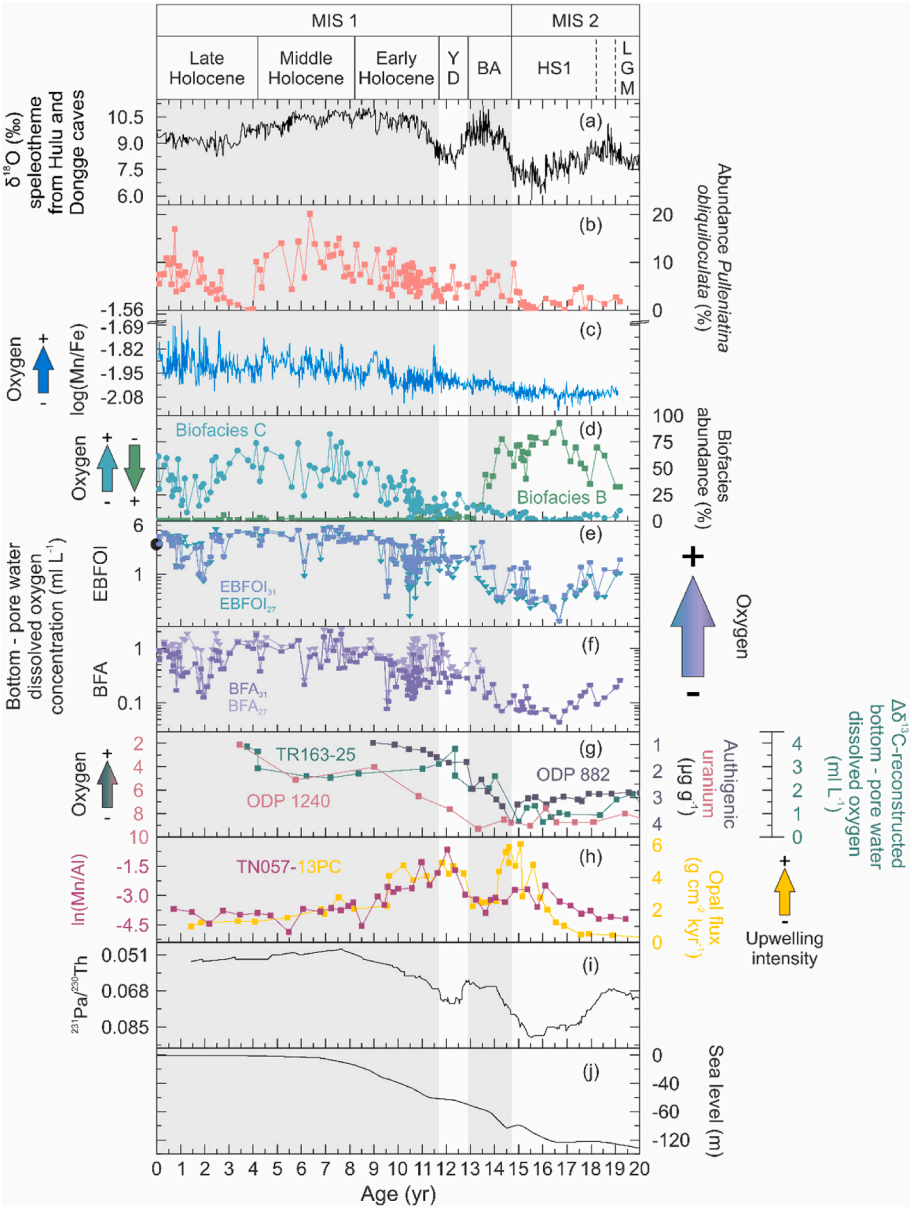

Fig. 7. Evolution of bottom – pore water oxygenation and the intensity of the Kuroshio Current: (a) $\delta^{18}O$ of speleothem from Hulu and Dongge caves (‰ VPDB, Cheng et al., 2016) (Fig. 1a); (b)–(f) data from core MD18-3523 (this study): (b) Pulleniatina obliquiloculata abundance (%); (c) log(Mn/Fe) ratio; (d) abundance of biofacies B (green dot) and C (light blue triangle) (%); (e to f) bottom – pore water dissolved oxygen concentration (ml L^{-1}) reconstructed using the Benthic Foraminifera Assemblage (BFA; Tetard et al., 2021) and the Enhanced Benthic Foraminifera Oxygen Index (EBFOI; Kranner et al., 2022), the transfer functions have been applied to the 31 taxa with an abundance greater than 5% in at least two samples ($EBFOI_{31}$ and BFA_{31}; dot), and to 27 of these 31 taxa by removing taxa from a different bathymetric region ($EBFOI_{27}$ and BFA_{27}; inverted triangle); (g) authigenic uranium concentration (µg g^{-1}) at ODP sites 882 (Jaccard et al., 2009) and 1240 (Jacobel et al., 2020) (Fig. 1a), and bottom – pore water dissolved oxygen concentration (ml L^{-1}) reconstructed using the $\Delta\delta^{13}C$ between deep infaunal and epifaunal benthic foraminifera (Hoogakker et al., 2015, 2018) (Fig. 1a), (h) ln(Mn/Al) ratio (Jaccard et al., 2016) and opal flux in core TN057-13 PC (Anderson et al., 2009) (Fig. 1a), (i) $^{231}Pa/^{230}Th$ shows changes in the intensity of the Atlantic Meridional Overturning Circulation (AMOC) (McManus et al., 2004a), (j) relative sea level (Lambeck et al., 2014). The black dot indicates the modern value (~3 ml L^{-1}) of oxygen concentration at 3000 m in the study zone (World Ocean Atlas, 2018; Garcia et al., 2019b). The marine isotope stages (MIS) are subdivided into millennial-scale periods with: Last Glacial Maximum (LGM), Heinrich Stadial 1 (HS1), Bølling-Allerød (BA), Younger Dryas (YD). Grey areas indicate warm periods. (For interpretation of the references to color in this figure legend, the reader is referred to the Web version of this article.)

Current bifurcation and therefore a slowdown of the Kuroshio Current (Hu et al., 2015; Qu and Lukas, 2003). Furthermore, the low sea level during HS1 (Fig. 7j) would have prevented the entry of the subsurface Ryukyu Current into the Okinawa Trough by the Yonaguni Depression, causing its deflection along the eastern edge of the Ryukyu Arc and the formation of an eastern branch of the Kuroshio Current (Fenies et al., 2023), probably further weakening the Kuroshio Current. After HS1, the intensification of the EASM (Cheng et al., 2016) and the establishment of La Niña-like conditions in the equatorial Pacific due to later summer – early autumn perihelion (Clement et al., 1999; Yu et al., 2023) would have led to a southward migration of the North Equatorial Current bifurcation and, consequently, to the intensification of the Kuroshio Current (Hu et al., 2015; Qu and Lukas, 2003). The rise of the sea level (Fig. 7j) would have caused the reentrance of the Ryukyu Current into the Okinawa Trough and the collapse of the Kuroshio Current eastern branch, contributing to the intensification of the Kuroshio Current main

stream (Fenies et al., 2023).

Previous studies have suggested a major influence of vertical mixing caused by the Kuroshio Current on the bottom – pore water oxygenation in the Okinawa Trough (Li et al., 2020; Lim et al., 2017; Vats et al., 2021; Zou et al., 2020, 2021). However, these studies are based on sediment cores collected at depths between 703 and 1421 m (Fig. 1b), whereas core MD18-3523 was taken at a depth of 2972 m. Thus, although there is a correlation between the abundance of *P. obliquiloculata* and oxygenation proxies, present-day measurements of the vertical mixing or hydrodynamic models are needed to fully assert the influence of the Kuroshio Current at a depth of nearly 3000 m.

The second regional mechanism is the intensification of the organic matter flux to the sea floor caused by an enhanced marine primary productivity during HS1, resulting in an increase in oxygen consumption through the degradation of organic matter, as evidenced by the high Br/Ti, TOC and BFAR values, and biofacies B abundance and faunal composition (Fig. 8e, g, 8h and 8j). The decline of Br/Ti and BFAR values, and biofacies B abundance at the beginning of the BA is concomitant with the weakening of the EAWM winds as recorded by the mean grain size data from the Gulang Loess (Sun et al., 2012) (Fig. 8b). During HS1, the cooling of the Northern Hemisphere, mainly due to the collapse of the AMOC (Fig. 7i), would have led to faster and more intense cooling of the Eurasian continent than of the North Pacific due to the difference in thermal inertia (Ruddiman, 2001; Sun et al., 2012). This would have resulted in an intensification of the Siberian High over the Eurasian continent (Huang et al., 2011; Sun et al., 2012; Yang et al., 2020) and of the Aleutian Low over the western North Pacific (McGee et al., 2018; Okumura et al., 2009; Wagner et al., 2010), causing the intensification of the EAWM.

This strengthening of the EAWM would have led to an increase in the surface wind stress over the subtropical western North Pacific (Sun et al., 2012) and carried mineral Fe from the hinterland to the oligotrophic waters of the North Pacific Subtropical Gyre during spring and summer (Mahowald et al., 2005; Wan et al., 2020; Wang and Ho, 2020; Zhong et al., 2022), as evidenced by the accumulation of dust and the concentration of soluble iron in core MD06-3024 (Fig. 8b), in the east of the Philippines (Fig. 1b) (Xu et al., 2015). In addition, the strengthening of the wind stress over the sea surface would have increased the water column vertical mixing (Hao et al., 2012; Steinke et al., 2010; Zhang et al., 2016) favoring the migration of the nutrient-rich Kuroshio Current intermediate water towards the surface (Chen et al., 2017, 2021, 2022). The combination of aeolian inputs of micronutrients i.e., iron, and increased level of macronutrients, nitrate and phosphate, by the deepening of the vertical mixing bringing nutrients from the subsurface upwards into the photic zone, would have provided particularly favorable conditions for marine primary productivity (Browning et al., 2022; Letelier et al., 2019; Prospero, 1990; Wang and Ho, 2020; Wen et al., 2022). This scenario is consistent with the previous observation of an increase in Br/Al, TOC, TN and $\delta^{13}C_{org}$ and decrease of $\delta^{15}N_{sed}$ during LGM and HS1 in nearby core MD18-3532 (Fenies et al., 2023).

After HS1, the weakening of the EAWM winds would have halted the supply of dust-borne iron and the upwelling of phosphate and nitrate from the Kuroshio Current subsurface waters, causing the decline of the marine primary productivity (Fig. 8e). The subsequent reduction of the organic matter flux would have resulted in a decrease in the consumption of bottom – pore water dissolved oxygen through the degradation of organic matter, causing the increase of the bottom – pore water oxygenation (Fig. 8i to l).

Overall, these results indicate an intensified marine biological pump under the influence of the EAWM in the northwestern Philippine Sea during HS1. They support a pronounced role of this region in the carbon storage during the beginning of the deglaciation (Fenies et al., 2023; Hu et al., 2021).

5.2. Changes in the terrestrial transfer to the ocean of carbon and impact on the carbon storage in marine sediments after the HS1

The period from 14.0 to (BA to Early Holocene) is marked by a halt in the increase of the bottom – pore water oxygenation (Fig. 7c to f and Fig. 8i to l). It might be attributed to the two-stage nature of the intensification of the AABW formation, with a first pulse during HS1 and a second one during YD (Fig. 7h), and the delay required for the ventilation from the second pulse to reach the study site (around 1 kyr at this time) (de la Fuente et al., 2015). However, as this phenomenon is not observed elsewhere in the North Pacific (Fig. 7g), we suggest that it is more likely to be linked to a local mechanism.

This period is marked by a substantial supply of terrestrial material and organic matter to the sea floor caused by strengthened erosion on Taiwan island as evidenced by the increase of Ti/K and the still high values of TOC during the BA and the peak at the beginning of the Early Holocene, while the marine primary productivity (Br/Ti) has already start to decline (Fig. 8d, e and 8g). The strengthening of the transfer of terrigenous material to the sea floor during this period is also shown by the still high values during the BA and the increase of the BFAR and biofacies A values, particularly of reworked taxa coming from the upper slope and other taxa abundance favoured by the large inputs of organic matter, possibly of continental origin, during the Early Holocene (Fig. 8f and h). This transfer of continental materials to the sea floor has been likely carried out either by turbidity currents resulting from slope destabilisation or hyperpycnal flows. The second are turbidity-like flows account for 30–42% of the sedimentary discharge from Taiwan to the ocean (Dadson et al., 2005) and transport terrestrial petrogenic and biospheric organic carbon to the seafloor (Hilton et al., 2008; Kao et al., 2010, 2014). The turbidity currents could also be the result of earthquake triggered slope failures affecting the submarine slope and more specifically the one at the vicinity of the river mouths. Indeed, coseismic turbidites have been documented over the last 2.7 kyr upslope (Lehu et al., 2016) and downslope (Ratzov et al., 2023) in the Nanao Basin. Those in the Nanao basin are particularly enriched in fresh continental organic matter (plant/wood debris) compared to the over- and under-lying deposits. These co-seismic deposits support a two-staged deposition: a first settling on the upper slope close the river mouths, then a slope failure evolving into turbidity currents. The time between the two stages is probably short, given the high seismicity in the studied area and the mean recurrence of 30–120 years of the co-seismic deposits (Ratzov et al., 2023) over the last 2kyr. The resulting influx of labile biospheric continental organic matter would have enhanced the consumption of bottom – pore water oxygenation through oxidation.

The strongest erosion of Taiwan during the BA and the Early Holocene is consistent with the records in Taiwan's terrestrial archives. Lake Dongyuan in southern Taiwan, presents an increase in the total carbon accumulation rate, the relative abundance of wood fragments and the decrease of the chemical index of alteration (CIA) (Ding et al., 2016b), a proxy that has recently been shown to be inversely correlated with physical erosion in Taiwan (Zheng et al., 2024). The end of the deglaciation is also marked by an increase in the occurrence of large landslides over Taiwan (Hsieh et al., 2011). The highest continental – ocean transfer during these periods is also coherent with the marine archives, as evidenced by the increase in sedimentation rate and export in fossil organic carbon in core MD01-2403 in the southern Okinawa Trough (Kao et al., 2008) (Fig. 1a), the increase in sedimentation rate and turbidite frequency in core MD10-3291 collected on a levee of the Gaoping Canyon, offshore south-western Taiwan (Yu et al., 2017) and the high carbonate dilution by large terrestrial input in the northern South China Sea (Huang et al., 2015). The strengthening in the erosion of Taiwan during the BA and the Early Holocene is likely to be related to an upsurge in precipitations due to the intensification of the EASM and in the intensity or frequency of the typhoons affecting Taiwan (Ding et al., 2016a, 2020). It is also possible that this period experienced higher seismic activity related to isostatic rebound following the retreat

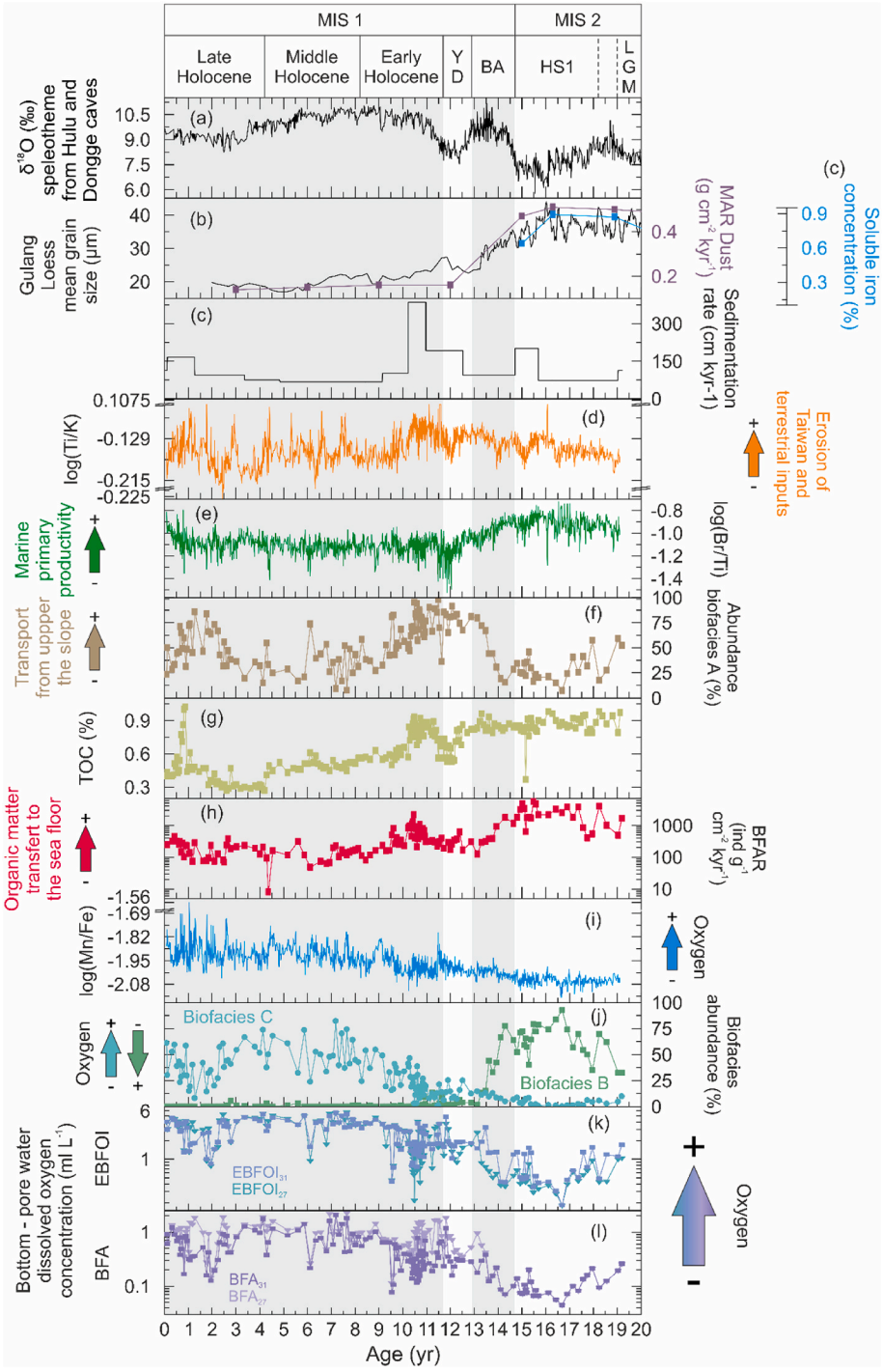

Fig. 8. Comparison of paleoproductivity records with (a) $\delta^{18}O$ of speleothem from Hulu and Dongge caves in per mille (‰) (Cheng et al., 2016) (Fig. 1a); (b) Gulang Loess mean grain size (μm) (Sun et al., 2012) (Fig. 1a), dust mass accumulation rate (MAR) and soluble iron concentration shows respectively the amount of dust (g cm^{-2} kyr^{-1}) and soluble iron (%) brought to the ocean from the Chinese Loess Plateau by the EAWM winds in core MD06-3047, east of the Philippines (Xu et al., 2015) (Fig. 1b); (c)–(l) data from core MD18-3523 (this study): (c) sedimentation rate (cm kyr^{-1}), (d) log(Ti/K) ratio, (e) log(Br/Ti), (f) abundance of the biofacies A (%), (g) total organic carbon (TOC, %), (h) Benthic Foraminifera Accumulation Rate (BFAR, ind g^{-1} cm^{-2} kyr^{-1}), (i) log(Mn/Fe) ratio, (j) abundance of biofacies B (green dot) and C (light blue triangle) (%); (k) bottom – pore water dissolved oxygen concentration (ml L^{-1}) reconstructed using the Benthic Foraminifera Assemblage (BFA; Tetard et al., 2021) and the Enhanced Benthic Foraminifera Oxygen Index (EBFOI; Kranner et al., 2022), the transfer functions have been applied to the 31 taxa with an abundance greater than 5% in at least two samples ($EBFOI_{31}$ and BFA_{31}; dot), and to 27 of these 31 taxa by removing taxa from a different bathymetric region ($EBFOI_{27}$ and BFA_{27}; inverted triangle). The marine isotope stages (MIS) are subdivided into millennial-scale periods with: Last Glacial Maximum (LGM), Heinrich Stadial 1 (HS1), Bølling-Allerød (BA), Younger Dryas (YD). Grey areas indicate warm periods. (For interpretation of the references to color in this figure legend, the reader is referred to the Web version of this article.)

of Taiwanese glaciers after the YD (Hebenstreit et al., 2011).

After 9 ka, at the end of the Early Holocene, the bottom-pore water oxygenation began to increase again, while the continent-ocean transfer of terrigenous material decreased (Fig. 8d and g), supporting the view that oxygen was consumed by the degradation of fresh terrestrial organic matter. The abundance of biofacies A, TOC and Ti/K reach a minimum from 4 to 2 ka, before showing an intense increase after 2 ka, also slightly reflected in the BFAR (Fig. 8d, f, 8g and 8h). This indicates a decrease in the erosion and transfer of continental material and organic matter to the deep ocean until the beginning of the Late Holocene, and an upsurge in these mechanisms after 2 ka. The progressive decrease of the transfer of continental organic matter during the Middle Holocene and the beginning of the Late Holocene led to a gradual increase in the bottom – pore water oxygenation over this period, reaching a maximum from 6 to 2 ka (Fig. 8i to l). This might have been caused by the decline in the EASM precipitations during the Holocene Thermal Maximum as recorded in Taiwan and southern China lakes (Ding et al., 2020; Wang, 2024). The reasons for the increase in dry conditions over this period are still debated but could be related to the meridional migration of the westerlies and the West Pacific Subtropical High due to changes in the inter-hemispheric temperature gradient (Ding et al., 2020).

After 2 ka, the rise in the erosion and continent – ocean transfer of organic matter resulted in a higher consumption of bottom – pore water dissolved oxygen through the degradation of the organic matter, as seen through the reduction in biofacies C abundance and the decline in the reconstructed bottom – pore water oxygenation, possibly reaching suboxic conditions (Fig. 8j to l). Like during the BA and Early Holocene, the increase in the erosion of Taiwan would have been related to an intensification of the EASM precipitations and rise in the intensity or frequency of typhoons affecting Taiwan, as evidenced by high sedimentation rate and low microfossil preservation in the Dahu Lake and Tsuifong Lake sediments (Wang et al., 2014), in diatom and pollen records in Tien pond sediments (Wang, 2024), in diatom, organic geochemical proxies, magnetic susceptibility and pollen records in Liyu Lake sediments (Wang et al., 2022) and numerous mass-wasting records in riverine fan terraces in the Pa-chang River catchment (Hsieh et al., 2014).

Overall, these results show an increase in the transfer and burial efficiency of particulate organic carbon in the deep ocean during the BA, the Early Holocene and the last 2 kyr of the Late Holocene (Fig. 8d and g). The partial degradation of the labile biospheric organic matter during these periods resulted in a reduction in bottom – pore water oxygenation (Fig. 8k to l), further favouring the conservation of the remaining organic matter. Unfortunately, our multiproxy datasets do not allow to measure the relative abundance of the biospheric and petrogenic components of the organic matter transferred to the ocean. It is particularly important because only the burial of terrestrial biospheric organic carbon in marine sediments by the turbidity pump will have an influence on the atmospheric CO_2 concentration. Indeed, its burial in marine sediments removes organic matter from the continent-atmosphere interface and prevents its respiration, which would cause the return of some of the carbon from organic matter to the atmosphere. On the other hand, the transport of terrestrial petrogenic carbon and its reburial in the marine sediments will not have any effect on the atmospheric CO_2 concentration as this carbon was already stored in rocks several million years ago (Talling et al., 2024). Worse, its degradation during the transport might result in a transformation of petrogenic carbon in CO_2, turning the continent-ocean transfer from a sink to a source of atmospheric CO_2. However, a recent study by Zheng et al. (2024) of surface and riverine sediments from Taiwan and a core located at the mouth of the Zhuoshui river, west of Taiwan, observes that the amount of biospheric organic carbon is logarithmically correlated with the amount of total organic carbon in soils of Taiwan and that this relationship is maintained during the continental-ocean transfer. Assuming that this relationship prevails for the whole of Taiwan, we suggest that the continental organic matter transferred to the ocean floor is mainly composed of biospheric organic carbon, turning the east coast of Taiwan into an atmospheric carbon sink thanks to an effective turbidity pump during the BA, the Early Holocene and the last 2 kyr of the Late Holocene. This observation is conflicting with the one made by Zheng et al. (2024) on the west coast of Taiwan, showing a more effective carbon turbidity pump during cold periods (LGM and YD) than during warm periods (BA and Holocene). These contradictory outcomes highlight a difference in the response of the east and west coasts to hydroclimatic changes in Taiwan, most likely related to the presence of the Central Mountain Range and by the difference in lithology and watershed morphology, the greater exposure to extreme events and precipitation, and the steeper slope gradient of Taiwan's east coast (Kao and Milliman, 2008), allowing better transfer of terrigenous material to the ocean during warm periods.

6. Conclusions

The purpose of this study was to investigate changes in the efficiency of the particulate organic carbon pump since the LGM in the northwestern Philippine Sea, East of Taiwan. Through the multiproxy study including benthic foraminiferal assemblages, organic and inorganic geochemistry and sedimentary proxies, we have been able to highlight the persistence of poor bottom – pore water oxygenation conditions at a depth of 3000 m during HS1 in this region. In addition, enhanced marine primary productivity is observed during HS1, most likely due to the intensification of the EAWM winds, bringing nutrients to the oligotrophic surface waters via dust and favouring the deepening of the vertical mixing of the water column. This configuration of poor bottom – pore water oxygenation and intense transfer of marine organic matter to the sea floor suggests increased effectiveness of marine biological pump during HS1. After HS1, the rise in the bottom – pore water oxygenation probably related to the global increase in AABW formation rate and the decline of the marine primary productivity caused by the decline in the intensity of the EAWM winds led to a reduced efficiency of the marine biological pump. During BA, the Early Holocene and the Late Holocene, the highest erosion of Taiwan caused by the increase of EASM precipitation and typhoon activity affecting Taiwan led to an increase of the continent to transfer of organic matter from the continent to the ocean and its burial in the marine sediments. This resulted in an effective carbon turbidity pump during these warm periods, specifically for the eastern part of Taiwan and contrary to the west coast of Taiwan that yields an effective carbon turbidity pump during cold periods (YD and LGM). This opposite behaviour highlight an east – west difference in the response and consequences of changes in Taiwan's past hydroclimate.

CRediT authorship contribution statement

Pierrick Fenies: Writing – original draft, Visualization, Methodology, Formal analysis, Conceptualization. **Maria-Angela Bassetti:** Writing – review & editing, Supervision, Project administration, Funding acquisition, Conceptualization. **Natalia Vazquez Riveiros:** Writing – review & editing, Supervision, Project administration, Conceptualization. **Sze Ling Ho:** Writing – review & editing, Investigation. **Yuan-Pin Chang:** Writing – review & editing, Investigation. **Ludvig Löwemark:** Writing – review & editing, Investigation. **Florian Bretonnière:** Investigation. **Nathalie Babonneau:** Writing – review & editing, Resources, Funding acquisition. **Gueorgui Ratzov:** Writing – review & editing, Resources, Funding acquisition. **Shu-Kun Hsu:** Writing – review & editing, Resources, Funding acquisition. **Chih-Chieh Su:** Writing – review & editing, Resources, Funding acquisition.

Declaration of competing interest

The authors declare that they have no known competing financial interests or personal relationships that could have appeared to influence the work reported in this paper.

Data availability

The data have been deposited on the Mendeley data platform and are available at the following link: https://data.mendeley.com/datasets/jyyny932fp/2

Acknowledgements

We would like to thank the crew and shipboard scientists of R/V *Marion* Dufresne during MD214/EAGER cruise, partially funded by the National Energy Program-Phase II (NEPII) project of Ministry of Science and Technology (MOST) of Taiwan and supported by the International Research Project (IRP): From Deep Earth to Extreme Events (D3E) between Centre National de la Recherche Scientifique (CNRS) of France and MOST of Taiwan. The authors acknowledge the CNRS INSU-SYSTER program for financial support through the ACTEE project. Löwemark acknowledges support from the Ministry of Science and Technology (MOST 111-2116-M-002-038-) and "The Featured Areas Research Center Program" within the framework of the Higher Education Sprout Project by the Ministry of Education in Taiwan. (NTU-111L901001). S.L. Ho acknowledges support from the Ministry of Science and Technology of Taiwan (MOST 107-2611-M-002-021-MY3). The authors would like to thank I. Ilkay (Bachelor student) and C. Latinis (MSc student) from the University of Perpignan for their respective contributions to the planktonic and benthic foraminifera analyses, and R.-Y. Tung (MSc student) and P.-T. Lee (PhD student) for their contribution to the picking of planktonic foraminifera for radiocarbon dating.

Appendix A. Supplementary data

Supplementary data to this article can be found online at https://doi.org/10.1016/j.qsa.2024.100223.

References

Altenbach, A.V., Pflaumann, U., Schiebel, R., Thies, A., Timm, S., Trauth, M., 1999. Scaling percentages and distributional patterns of benthic foraminifera with flux rates of organic carbon. J. Foraminifer. Res. 29, 173–185.

Anderson, R.F., Ali, S., Bradtmiller, L.I., Nielsen, S.H.H., Fleisher, M.Q., Anderson, B.E., Burckle, L.H., 2009. Wind-driven upwelling in the Southern Ocean and the deglacial rise in atmospheric CO2. Science 323, 1443–1448. https://doi.org/10.1126/science.1167441.

Angue Minto'o, C.M., Bassetti, M.A., Morigi, C., Ducassou, E., Toucanne, S., Jouet, G., Mulder, T., 2015. Levantine intermediate water hydrodynamic and bottom water ventilation in the northern Tyrrhenian Sea over the past 56,000 years: new insights from benthic foraminifera and ostracods. Quaternary International, Correlations of Quaternary Fluvial, Eolian, Deltaic and Marine Sequences: SEQS 357, 295–313. https://doi.org/10.1016/j.quaint.2014.11.038, 2013.

Babonneau, N., Ratzov, G., 2018. MD 214/EAGER cruise,Marion Dufresne R/V. https://doi.org/10.17600/18000520.

Baohua, L., Zhimin, J., Pinxian, W., 1997. Pulleniatina obliquiloculata as a paleoceanographic indicator in the southern Okinawa trough during the last 20,000 years. Mar. Micropaleontol. 32, 59–69. https://doi.org/10.1016/S0377-8398(97)00013-3.

Barbieri, R., 1991. Phenotypic variation in gyroidinoides altiformis (stewart & stewart) and gyroidinoides subangulatus (plummer) (foraminifera). J. Micropalaeontol. 9, 233–238. https://doi.org/10.1144/jm.9.2.233.

Bauer, J.E., Cai, W.-J., Raymond, P.A., Bianchi, T.S., Hopkinson, C.S., Regnier, P.A.G., 2013. The changing carbon cycle of the coastal ocean. Nature 504, 61–70. https://doi.org/10.1038/nature12857.

Belanger, C.L., Sharon, Du, J., Payne, C.R., Mix, A.C., 2020. North Pacific deep-sea ecosystem responses reflect post-glacial switch to pulsed export productivity, deoxygenation, and destratification. Deep Sea Res. Oceanogr. Res. Pap. 164, 103341 https://doi.org/10.1016/j.dsr.2020.103341.

Bernhard, J.M., Sen Gupta, B.K., Borne, P.F., 1997. Benthic foraminiferal proxy to estimate dysoxic bottom-water oxygen concentrations; Santa Barbara Basin, U.S. Pacific continental margin. J. Foraminifer. Res. 27, 301–310. https://doi.org/10.2113/gsjfr.27.4.301.

Bertrand, S., Tjallingii, R., Kylander, M.E., Wilhelm, B., Roberts, S.J., Arnaud, F., Brown, E., Bindler, R., 2024. Inorganic geochemistry of lake sediments: a review of analytical techniques and guidelines for data interpretation. Earth Sci. Rev. 249, 104639 https://doi.org/10.1016/j.earscirev.2023.104639.

Boltovskoy, E., Giussani, G., Watanabe, S., Wright, R., 1980. Atlas of Benthic Shelf Foraminifera of the Southwest Atlantic. Springer, Netherlands, Dordrecht. https://doi.org/10.1007/978-94-009-9188-0.

Bouttes, N., Paillard, D., Roche, D.M., 2010. Impact of brine-induced stratification on the glacial carbon cycle. Clim. Past 6, 575–589. https://doi.org/10.5194/cp-6-575-2010.

Browning, T.J., Liu, X., Zhang, R., Wen, Z., Liu, J., Zhou, Y., Xu, F., Cai, Y., Zhou, K., Cao, Z., Zhu, Y., Shi, D., Achterberg, E.P., Dai, M., 2022. Nutrient co-limitation in the subtropical northwest pacific. Limnology and Oceanography Letters 7, 52–61. https://doi.org/10.1002/lol2.10205.

Cage, A.G., Pieńkowski, A.J., Jennings, A., Knudsen, K.L., Seidenkrantz, M.-S., 2021. Comparative analysis of six common foraminiferal species of the genera Cassidulina, Paracassidulina, and Islandiella from the Arctic–North Atlantic domain. J. Micropalaeontol. 40, 37–60. https://doi.org/10.5194/jm-40-37-2021.

Cannariato, K.G., Kennett, J.P., Behl, R.J., 1999. Biotic response to late Quaternary rapid climate switches in Santa Barbara Basin: ecological and evolutionary implications. Geology 27, 63–66. https://doi.org/10.1130/0091-7613(1999)027<0063:BRTLQR>2.3.CO;2.

Caralp, M., 1989. Abundance of Bulimina exilis and Melonis barleeanum: relationship to the quality of marine organic matter. Geo Mar. Lett. 9, 37–43.

Cartapanis, O., Bianchi, D., Jaccard, S.L., Galbraith, E.D., 2016. Global pulses of organic carbon burial in deep-sea sediments during glacial maxima. Nat. Commun. 7, 10796 https://doi.org/10.1038/ncomms10796.

Caulle, C., Koho, K.A., Mojtahid, M., Reichart, G.J., Jorissen, F.J., 2014. Live (Rose Bengal stained) foraminiferal faunas from the northern Arabian Sea: faunal succession within and below the OMZ. Biogeosciences 11, 1155–1175. https://doi.org/10.5194/bg-11-1155-2014.

Chan, S.A., Bălc, R., Humphrey, J.D., Amao, A.O., Kaminski, M.A., Alzayer, Y., Duque, F., 2022. Changes in paleoenvironmental conditions during the Late Jurassic of the western Neo-Tethys: calcareous nannofossils and geochemistry. Mar. Micropaleontol. 173, 102116 https://doi.org/10.1016/j.marmicro.2022.102116.

Chang, A.S., Pedersen, T.F., Hendy, I.L., 2014. Effects of productivity, glaciation, and ventilation on late Quaternary sedimentary redox and trace element accumulation on the Vancouver Island margin, western Canada. Paleoceanography 29, 730–746. https://doi.org/10.1002/2013PA002581.

Chauhan, T., Rasmussen, T.L., Noormets, R., 2016. Palaeoceanography of the Barents Sea continental margin, north of Nordaustlandet, Svalbard, during the last 74 ka. Boreas 45, 76–99. https://doi.org/10.1111/bor.12135.

Chen, C.-C., Jan, S., Kuo, T.-H., Li, S.-Y., 2017. Nutrient flux and transport by the Kuroshio east of Taiwan. J. Mar. Syst. 167, 43–54. https://doi.org/10.1016/j.jmarsys.2016.11.004.

Chen, C.-C., Lu, C.-Y., Jan, S., Hsieh, C., Chung, C.-C., 2022. Effects of the coastal uplift on the Kuroshio ecosystem, eastern taiwan, the western boundary current of the North Pacific Ocean. Front. Mar. Sci. 9, 796187 https://doi.org/10.3389/fmars.2022.796187.

Chen, C.-S., Chen, Y.-L., 2003. The rainfall characteristics of taiwan. Mon. Weather Rev. 131, 1323–1341. https://doi.org/10.1175/1520-0493(2003)131<1323:TRCOT>2.0.CO;2.

Chen, C.-T.A., Huang, T.-H., Wu, C.-H., Yang, H., Guo, X., 2021. Variability of the nutrient stream near Kuroshio's origin. Sci. Rep. 11, 5080. https://doi.org/10.1038/s41598-021-84420-5.

Cheng, H., Edwards, R.L., Sinha, A., Spötl, C., Yi, L., Chen, S., Kelly, M., Kathayat, G., Wang, X., Li, X., Kong, X., Wang, Y., Ning, Y., Zhang, H., 2016. The Asian monsoon over the past 640,000 years and ice age terminations. Nature 534, 640–646. https://doi.org/10.1038/nature18591.

Chiang, C.-S., Yu, H.-S., 2022. Controls of submarine canyons connected to shore during the LGM sea-level rise: examples from taiwan. J. Mar. Sci. Eng. 10, 494.

Clark, P.U., Shakun, J.D., Baker, P.A., Bartlein, P.J., Brewer, S., Brook, E., Carlson, A.E., Cheng, H., Kaufman, D.S., Liu, Z., 2012. Global climate evolution during the last deglaciation. Proc. Natl. Acad. Sci. USA 109, E1134–E1142. https://doi.org/10.1073/pnas.1116619109.

Clement, A.C., Seager, R., Cane, M.A., 1999. Orbital controls on the El niño/southern oscillation and the tropical climate. Paleoceanography 14, 441–456. https://doi.org/10.1029/1999PA900013.

Collen, J., Newell, P., 1999. Fissurina as an ectoparasite. J. Micropalaeontolgy 18, 110.

Cook, M.S., Ravelo, A.C., Mix, A., Nesbitt, I.M., Miller, N.V., 2016. Tracing subarctic Pacific water masses with benthic foraminiferal stable isotopes during the LGM and late Pleistocene. Deep-Sea Res. Part II: Topical Studies in Oceanography, Plio-Pleistocene Paleoceanography of the Bering Sea 125–126, 84–95. https://doi.org/10.1016/j.dsr2.2016.02.006.

Courtillat, M., Hallenberger, M., Bassetti, M.-A., Aubert, D., Jeandel, C., Reuning, L., Korpanty, C., Moissette, P., Mounic, S., Saavedra-Pellitero, M., 2020. New record of dust input and provenance during glacial periods in western Australia shelf (IODP expedition 356, site U1461) from the middle to late pleistocene. Atmosphere 11, 1251. https://doi.org/10.3390/atmos11111251.

Croudace, I.W., Rindby, A., Rothwell, R.G., 2006. ITRAX: Description and Evaluation of a New Multi-Function X-Ray Core Scanner, vol. 267. Geological Society, London, Special Publications, pp. 51–63. https://doi.org/10.1144/GSL.SP.2006.267.01.04.

Culver, S.J., 1988. New foraminiferal depth zonation of the northwestern Gulf of Mexico. Palaios 69–85.

Cushman, J.A., 1933. An Illustrated Key to the Genera of the Foraminifera. Norwood Press.

Dadson, S., Hovius, N., Pegg, S., Dade, W.B., Horng, M.J., Chen, H., 2005. Hyperpycnal river flows from an active mountain belt. J. Geophys. Res.: Earth Surf. 110, F04016 https://doi.org/10.1029/2004JF000244.

Dadson, S.J., Hovius, N., Chen, H., Dade, W.B., Hsieh, M.-L., Willett, S.D., Hu, J.-C., Horng, M.-J., Chen, M.-C., Stark, C.P., Lague, D., Lin, J.-C., 2003. Links between erosion, runoff variability and seismicity in the Taiwan orogen. Nature 426, 648–651. https://doi.org/10.1038/nature02150.

Das, M., Singh, R.K., Gupta, A.K., Bhaumik, A.K., 2017. Holocene strengthening of the Oxygen Minimum Zone in the northwestern Arabian Sea linked to changes in intermediate water circulation or Indian monsoon intensity? Palaeogeography, Palaeoclimatology, Palaeoecology, Development, evaluation and application of marine paleoclimatic/paleoceanographic proxies: Update 483, 125–135. https://doi.org/10.1016/j.palaeo.2016.10.035.

de Boer, A.M., Sigman, D.M., Toggweiler, J.R., Russell, J.L., 2007. Effect of global ocean temperature change on deep ocean ventilation. Paleoceanography 22. https://doi.org/10.1029/2005PA001242.

de la Fuente, M., Skinner, L., Calvo, E., Pelejero, C., Cacho, I., 2015. Increased reservoir ages and poorly ventilated deep waters inferred in the glacial Eastern Equatorial Pacific. Nat. Commun. 6, 7420. https://doi.org/10.1038/ncomms8420.

De Rijk, S., Jorissen, F.J., Rohling, E.J., Troelstra, S.R., 2000. Organic flux control on bathymetric zonation of Mediterranean benthic foraminifera. Mar. Micropaleontol. 40, 151–166. https://doi.org/10.1016/S0377-8398(00)00037-2.

De, S., Gupta, A.K., 2010. Deep-sea faunal provinces and their inferred environments in the Indian Ocean based on distribution of Recent benthic foraminifera. Palaeogeogr. Palaeoclimatol. Palaeoecol. 291, 429–442. https://doi.org/10.1016/j.palaeo.2010.03.012.

Denton, G.H., Anderson, R.F., Toggweiler, J.R., Edwards, R.L., Schaefer, J.M., Putnam, A. E., 2010. The last glacial termination. Science 328, 1652–1656. https://doi.org/10.1126/science.1184119.

Derrieux, F., Siame, L.L., Bourlès, D.L., Chen, R.-F., Braucher, R., Léanni, L., Lee, J.-C., Chu, H.-T., Byrne, T.B., 2014. How fast is the denudation of the Taiwan mountain belt? Perspectives from in situ cosmogenic 10Be. J. Asian Earth Sci. 88, 230–245. https://doi.org/10.1016/j.jseaes.2014.03.012.

Dessandier, P.-A., Bonnin, J., Kim, J.-H., Bichon, S., Grémare, A., Deflandre, B., de Stigter, H., Malaizé, B., 2015. Lateral and vertical distributions of living benthic foraminifera off the Douro River (western Iberian margin): impact of the organic matter quality. Mar. Micropaleontol. 120, 31–45. https://doi.org/10.1016/j.marmicro.2015.09.002.

DeVries, T., 2022. The Ocean carbon cycle. Annu. Rev. Environ. Resour. 47, 317–341. https://doi.org/10.1146/annurev-environ-120920-111307.

Dezileau, L., Lehu, R., Lallemand, S., Hsu, S.-K., Babonneau, N., Ratzov, G., Lin, A.T., Dominguez, S., 2016. Historical reconstruction of submarine earthquakes using ^{210}Pb, ^{137}Cs, and ^{241}Am turbidite chronology and radiocarbon reservoir age estimation off east taiwan. Radiocarbon 58, 25–36. https://doi.org/10.1017/RDC.2015.3.

Ding, X., Li, D., Zheng, L., Bao, H., Chen, H.-F., Kao, S.-J., 2016a. Sulfur geochemistry of a lacustrine record from taiwan reveals enhanced marine aerosol input during the early Holocene. Sci. Rep. 6, 38989 https://doi.org/10.1038/srep38989.

Ding, X., Zheng, L., Li, D., Yang, T.-N., Lee, T.-Q., Kao, S.-J., 2016b. Lacustrine record of centennial- and millennial-scale rainfall variability of the East Asian summer monsoon during the last deglaciation: multi-proxy evidence from Taiwan. Palaeogeogr. Palaeoclimatol. Palaeoecol. 450, 38–49. https://doi.org/10.1016/j.palaeo.2016.02.048.

Ding, X., Zheng, L., Zheng, X., Kao, S.-J., 2020. Holocene East asian summer monsoon rainfall variability in taiwan. Front. Earth Sci. 8, 234. https://doi.org/10.3389/feart.2020.00234.

Du, J., Mix, A.C., Haley, B.A., Belanger, C.L., Sharon, 2022. Volcanic trigger of ocean deoxygenation during Cordilleran ice sheet retreat. Nature 611, 74–80. https://doi.org/10.1038/s41586-022-05267-y.

Duchemin, G., Fontanier, C., Jorissen, F.J., Barras, C., Griveaud, C., 2007. Living small-sized (63–150 μm) foraminifera from mid-shelf to mid-slope environments in the Bay of Biscay. J. Foraminifer. Res. 37, 12–32. https://doi.org/10.2113/gsjfr.37.1.12.

Duplessy, J.C., Shackleton, N.J., Fairbanks, R.G., Labeyrie, L., Oppo, D., Kallel, N., 1988. Deepwater source variations during the last climatic cycle and their impact on the global deepwater circulation. Paleoceanography 3, 343–360. https://doi.org/10.1029/PA003i003p00343.

Duros, P., Fontanier, C., Metzger, E., Pusceddu, A., Cesbron, F., de Stigter, H.C., Bianchelli, S., Danovaro, R., Jorissen, F.J., 2011. Live (stained) benthic foraminifera in the whittard canyon, celtic margin (NE atlantic). Deep Sea Res. Oceanogr. Res. Pap. 58, 128–146. https://doi.org/10.1016/j.dsr.2010.11.008.

Enge, A.J., Kucera, M., Heinz, P., 2012. Diversity and microhabitats of living benthic foraminifera in the abyssal Northeast Pacific. Mar. Micropaleontol. 96 (97), 84–104. https://doi.org/10.1016/j.marmicro.2012.08.004.

Erdem, Z., Schönfeld, J., Rathburn, A.E., Pérez, M.-E., Cardich, J., Glock, N., 2020. Bottom-water deoxygenation at the Peruvian margin during the last deglaciation recorded by benthic foraminifera. Biogeosciences 17, 3165–3182. https://doi.org/10.5194/bg-17-3165-2020.

Fanget, A.-S., Bassetti, M.-A., Fontanier, C., Tudryn, A., Berné, S., 2016. Sedimentary archives of climate and sea-level changes during the Holocene in the Rhône prodelta (NW Mediterranean Sea). Clim. Past 12, 2161–2179. https://doi.org/10.5194/cp-12-2161-2016.

Fenies, P., 2023. Changements paléocéanographiques et enregistrement des évènements extrêmes dans les archives sédimentaires marines depuis le dernier maximum glaciaire à l'Est de Taiwan. PhD Thesis. Université de Perpignan, p. 368p.

Fenies, P., Bassetti, M.-A., Riveiros, N.V., Menniti, C., Frigola, C., Babonneau, N., Ratzov, G., Hsu, S.-K., Su, C.-C., 2023. Changes in Kuroshio Current dynamics and East Asian monsoon variability during the last 26 kyr. Palaeogeogr. Palaeoclimatol. Palaeoecol. 632, 111836 https://doi.org/10.1016/j.palaeo.2023.111836.

Ferreira, D., Cessi, P., Coxall, H.K., de Boer, A., Dijkstra, H.A., Drijfhout, S.S., Eldevik, T., Harnik, N., McManus, J.F., Marshall, D.P., Nilsson, J., Roquet, F., Schneider, T., Wills, R.C., 2018. Atlantic-pacific asymmetry in deep water formation. Annu. Rev. Earth Planet Sci. 46, 327–352. https://doi.org/10.1146/annurev-earth-082517-010045.

Fiorini, F., 2015. Recent benthic foraminifera from the Caribbean continental slope and shelf off west of Colombia. J. S. Am. Earth Sci. 60, 117–128. https://doi.org/10.1016/j.jsames.2015.03.003.

Fontanier, C., Biscara, L., Mamo, B., Delord, E., 2015. Deep-sea benthic foraminifera in an area around the Cassidaigne Canyon (NW Mediterranean) affected by bauxite discharges. Mar. Biodivers. 45, 371–382. https://doi.org/10.1007/s12526-014-0281-9.

Fontanier, C., Jorissen, F.J., Chaillou, G., Anschutz, P., Grémare, A., Griveaud, C., 2005. Live foraminiferal faunas from a 2800 m deep lower canyon station from the Bay of Biscay: faunal response to focusing of refractory organic matter. Deep Sea Res. Oceanogr. Res. Pap. 52, 1189–1227. https://doi.org/10.1016/j.dsr.2005.01.006.

Fontanier, C., Jorissen, F.J., Chaillou, G., David, C., Anschutz, P., Lafon, V., 2003. Seasonal and interannual variability of benthic foraminiferal faunas at 550m depth in the Bay of Biscay. Deep Sea Res. Oceanogr. Res. Pap. 50, 457–494. https://doi.org/10.1016/S0967-0637(02)00167-X.

Fontanier, C., Jorissen, F.J., Lansard, B., Mouret, A., Buscail, R., Schmidt, S., Kerhervé, P., Buron, F., Zaragosi, S., Hunault, G., Ernoult, E., Artero, C., Anschutz, P., Rabouille, C., 2008. Live foraminifera from the open slope between grand rhône and petit rhône canyons (Gulf of lions, NW mediterranean). Deep Sea Res. Oceanogr. Res. Pap. 55, 1532–1553. https://doi.org/10.1016/j.dsr.2008.07.003.

Fuhr, M., Laukert, G., Yu, Y., Nürnberg, D., Frank, M., 2021. Tracing water mass mixing from the equatorial to the North Pacific Ocean with dissolved neodymium isotopes and concentrations. Front. Mar. Sci. 7, 1261. https://doi.org/10.3389/fmars.2020.603761.

Galbraith, E.D., Jaccard, S.L., Pedersen, T.F., Sigman, D.M., Haug, G.H., Cook, M., Southon, J.R., Francois, R., 2007. Carbon dioxide release from the North Pacific abyss during the last deglaciation. Nature 449, 890–893. https://doi.org/10.1038/nature06227.

Garcia, H., Weathers, K., Paver, C., Smolyar, I., Boyer, T., Locarnini, M., Zweng, M., Mishonov, A., Baranova, O., Seidov, D., Reagan, J., 2019a. World Ocean Atlas 2018. Vol. 4: Dissolved Inorganic Nutrients (Phosphate, Nitrate and Nitrate+nitrite, Silicate).

Garcia, H., Weathers, K., Paver, C., Smolyar, I., Boyer, T., Locarnini, M., Zweng, M., Mishonov, A., Baranova, O., Seidov, D., Reagan, J., 2019b. World Ocean Atlas 2018, Volume 3: Dissolved Oxygen, Apparent Oxygen Utilization, and Dissolved Oxygen Saturation.

Geslin, E., Heinz, P., Jorissen, F., Hemleben, Ch, 2004. Migratory responses of deep-sea benthic foraminifera to variable oxygen conditions: laboratory investigations. Mar. Micropaleontol. 53, 227–243. https://doi.org/10.1016/j.marmicro.2004.05.010.

Glock, N., 2023. Benthic foraminifera and gromiids from oxygen-depleted environments – survival strategies, biogeochemistry and trophic interactions. Biogeosciences 20, 3423–3447. https://doi.org/10.5194/bg-20-3423-2023.

Goineau, A., Fontanier, C., Jorissen, F.J., Lansard, B., Buscail, R., Mouret, A., Kerhervé, P., Zaragosi, S., Ernoult, E., Artéro, C., Anschutz, P., Metzger, E., Rabouille, C., 2011. Live (stained) benthic foraminifera from the Rhône prodelta (Gulf of Lion, NW Mediterranean): environmental controls on a river-dominated shelf. J. Sea Res. 65, 58–75. https://doi.org/10.1016/j.seares.2010.07.007.

Goineau, A., Fontanier, C., Mojtahid, M., Fanget, A.-S., Bassetti, M.-A., Berné, S., Jorissen, F., 2015. Live–dead comparison of benthic foraminiferal faunas from the Rhône prodelta (Gulf of Lions, NW Mediterranean): development of a proxy for palaeoenvironmental reconstructions. Mar. Micropaleontol. 119, 17–33. https://doi.org/10.1016/j.marmicro.2015.07.002.

Gong, X., Lembke-Jene, L., Lohmann, G., Knorr, G., Tiedemann, R., Zou, J.J., Shi, X.F., 2019. Enhanced North Pacific deep-ocean stratification by stronger intermediate water formation during Heinrich Stadial 1. Nat. Commun. 10, 656. https://doi.org/10.1038/s41467-019-08606-2.

Gooday, A.J., 2003. Benthic Foraminifera (Protista) as Tools in Deep-Water Palaeoceanography: Environmental Influences on Faunal Characteristics.

Gooday, A.J., 1988. A response by benthic Foraminifera to the deposition of phytodetritus in the deep sea. Nature 332, 70–73. https://doi.org/10.1038/332070a0.

Gooday, A.J., Jorissen, F.J., 2012. Benthic foraminiferal biogeography: controls on global distribution patterns in deep-water settings. Ann. Rev. Mar. Sci 4, 237–262. https://doi.org/10.1146/annurev-marine-120709-142737.

Gooday, A.J., Malzone, M.G., Bett, B.J., Lamont, P.A., 2010. Decadal-scale changes in shallow-infaunal foraminiferal assemblages at the porcupine abyssal plain, NE atlantic. Deep-Sea Res. Part II: Topical Studies in Oceanography, Water Column and Seabed Studies at the PAP Sustained Observatory in the Northeast Atlantic 57, 1362–1382. https://doi.org/10.1016/j.dsr2.2010.01.012.

Guo, Y., 1991. The Kuroshio. Part II. Primary productivity and phytoplankton. Oceanogr. Mar. Biol. Annu. Rev. 29, 155–189.

Haller, C., Hallock, P., Hine, A.C., Smith, C.G., 2018. Benthic foraminifera from the carnarvon ramp reveal variability in leeuwin current activity (western Australia) since the pliocene. Mar. Micropaleontol. 142, 25–39. https://doi.org/10.1016/j.marmicro.2018.05.005.

Hanagata, S., Nobuhara, T., 2015. Illustrated guide to pliocene foraminifera from miyakojima, Ryukyu island arc, with comments on biostratigraphy. Palaeontol. Electron. 1, 1–140. https://doi.org/10.26879/444.

Hansell, D.A., Carlson, C.A., Repeta, D.J., Schlitzer, R., 2009. Dissolved organic matter in the ocean: a controversy stimulates new insights. Oceanography 22, 202–211.

Hao, J., Chen, Y., Wang, F., Lin, P., 2012. Seasonal thermocline in the China Seas and northwestern Pacific Ocean: seasonal thermocline in China seas. J. Geophys. Res. 117, C02022 https://doi.org/10.1029/2011JC007246.

Haynes, J.R., 1981. Foraminifera. Springer.

Hayward, B.W., Carter, R., Grenfell, H.R., Hayward, J.J., 2001. Depth distribution of Recent deep-sea benthic foraminifera east of New Zealand, and their potential for improving paleobathymetric assessments of Neogene microfaunas. N. Z. J. Geol. Geophys 44, 555–587.
Hayward, B.W., Coze, F.L., Vandepitte, L., Vanhoorne, B., 2020. Foraminifera in the world register of marine species (worms) taxonomic database. J. Foraminifer. Res. 50, 291–300. https://doi.org/10.2113/gsjfr.50.3.291.
Heaton, T.J., Köhler, P., Butzin, M., Bard, E., Reimer, R.W., Austin, W.E.N., Bronk Ramsey, C., Grootes, P.M., Hughen, K.A., Kromer, B., Reimer, P.J., Adkins, J., Burke, A., Cook, M.S., Olsen, J., Skinner, L.C., 2020. Marine20—the marine radiocarbon age calibration curve (0–55,000 cal BP). Radiocarbon 62, 779–820. https://doi.org/10.1017/RDC.2020.68.
Hebenstreit, R., Ivy-Ochs, S., Kubik, P.W., Schlüchter, C., Böse, M., 2011. Lateglacial and early Holocene surface exposure ages of glacial boulders in the Taiwanese high mountain range. Quat. Sci. Rev. 30, 298–311. https://doi.org/10.1016/j.quascirev.2010.11.002.
Herguera, J.C., 2000. Last glacial paleoproductivity patterns in the eastern equatorial Pacific: benthic foraminifera records. Mar. Micropaleontol. 40, 259–275. https://doi.org/10.1016/S0377-8398(00)00041-4.
Herguera, J.C., 1992. Deep-sea benthic foraminifera and biogenic opal: glacial to postglacial productivity changes in the western equatorial Pacific. Marine Micropaleontology, Approaches to Paleoproductivity Reconstructions 19, 79–98. https://doi.org/10.1016/0377-8398(92)90022-C.
Herguera, J.C., Berger, W.H., 1991. Paleoproductivity from benthic foraminifera abundance: glacial to postglacial change in the west-equatorial Pacific. Geology 19, 1173–1176. https://doi.org/10.1130/0091-7613(1991)019<1173:PFBFAG>2.3.CO;2.
Hess, S., Jorissen, F.J., Venet, V., Abu-Zied, R., 2005. Benthic foraminiferal recovery after recent turbidite deposition in Cap Breton Canyon, Bay of Biscay. J. Foraminifer. Res. 35, 114–129. https://doi.org/10.2113/35.2.114.
Hill, M.O., Gauch, H.G., 1980. Detrended correspondence analysis: an improved ordination technique. Vegetatio 42, 47–58. https://doi.org/10.1007/BF00048870.
Hilton, R.G., 2017. Climate regulates the erosional carbon export from the terrestrial biosphere. Geomorphology, Connectivity in Geomorphology from Binghamton 277, 118–132. https://doi.org/10.1016/j.geomorph.2016.03.028, 2016.
Hilton, R.G., Galy, A., Hovius, N., Chen, M.-C., Horng, M.-J., Chen, H., 2008. Tropical-cyclone-driven erosion of the terrestrial biosphere from mountains. Nat. Geosci. 1, 759–762. https://doi.org/10.1038/ngeo333.
Hilton, R.G., Galy, A., Hovius, N., Horng, M.-J., Chen, H., 2010. The isotopic composition of particulate organic carbon in mountain rivers of Taiwan. Geochem. Cosmochim. Acta 74, 3164–3181. https://doi.org/10.1016/j.gca.2010.03.004.
Hilton, R.G., Galy, A., Hovius, N., Kao, S.-J., Horng, M.-J., Chen, H., 2012. Climatic and geomorphic controls on the erosion of terrestrial biomass from subtropical mountain forest. Global Biogeochem. Cycles 26. https://doi.org/10.1029/2012GB004314.
Holbourn, A.E., Henderson, A.S., 2002. Re-illustration and revised taxonomy for selected deep-sea benthic foraminifers. Palaeontol. Electron. 4, 34.
Holbourn, A.E., Henderson, A.S., MacLeod, N., MacLeod, N., 2013. Atlas of Benthic Foraminifera. Wiley Online Library.
Hoogakker, B.A.A., Elderfield, H., Schmiedl, G., McCave, I.N., Rickaby, R.E.M., 2015. Glacial–interglacial changes in bottom-water oxygen content on the Portuguese margin. Nat. Geosci. 8, 40–43. https://doi.org/10.1038/ngeo2317.
Hoogakker, B.A.A., Lu, Z., Umling, N., Jones, L., Zhou, X., Rickaby, R.E.M., Thunell, R., Cartapanis, O., Galbraith, E., 2018. Glacial expansion of oxygen-depleted seawater in the eastern tropical Pacific. Nature 562, 410–413. https://doi.org/10.1038/s41586-018-0589-x.
Horikawa, K., Kozaka, Y., Okazaki, Y., Sagawa, T., Onodera, J., Asahi, H., Shin, K.-C., Asahara, Y., Takahashi, K., 2021. Neodymium isotope records from the northwestern pacific: implication for deepwater ventilation at Heinrich stadial 1. Paleoceanogr. Paleoclimatol. 36, e2021PA004312 https://doi.org/10.1029/2021PA004312.
Hsieh, M.-L., Ching, K.-E., Chyi, S.-J., Kang, S.-C., Chou, C.-Y., 2014. Late Quaternary mass-wasting records in the actively uplifting Pa-chang catchment, southwestern Taiwan. Geomorphology 216, 125–140. https://doi.org/10.1016/j.geomorph.2014.03.040.
Hsieh, M.-L., Liew, P.-M., Chen, H.-W., 2011. Early Holocene catastrophic mass-wasting event and fan-delta development on the Hua-tung coast, eastern Taiwan. Geomorphology 134, 378–393. https://doi.org/10.1016/j.geomorph.2011.07.012.
Hsiung, K.-H., Kanamatsu, T., Ikehara, K., Shiraishi, K., Horng, C.-S., Usami, K., 2017. Morpho-sedimentary features and sediment dispersal systems of the southwest end of the Ryukyu Trench: a source-to-sink approach. Geo Mar. Lett. 37, 561–577. https://doi.org/10.1007/s00367-017-0509-3.
Hu, D., Wu, L., Cai, W., Gupta, A.S., Ganachaud, A., Qiu, B., Gordon, A.L., Lin, X., Chen, Z., Hu, S., Wang, G., Wang, Q., Sprintall, J., Qu, T., Kashino, Y., Wang, F., Kessler, W.S., 2015. Pacific western boundary currents and their roles in climate. Nature 522, 299–308. https://doi.org/10.1038/nature14504.
Hu, Z., Huang, B.-Q., Liu, L.-J., Wang, N., 2021. Spatiotemporal patterns of sediment deposition on the northern slope of the South China Sea in the last 150,000 years. J. Palaeogeogr. 10, 21. https://doi.org/10.1186/s42501-021-00102-3.
Huang, E., Tian, J., Qiao, P., Wan, S., Xie, X., Yang, W., 2015. Early interglacial carbonate-dilution events in the South China Sea: implications for strengthened typhoon activities over subtropical East Asia. Quat. Sci. Rev. 125, 61–77. https://doi.org/10.1016/j.quascirev.2015.08.007.
Huang, E., Tian, J., Steinke, S., 2011. Millennial-scale dynamics of the winter cold tongue in the southern South China Sea over the past 26ka and the East Asian winter monsoon. Quat. Res. 75, 196–204. https://doi.org/10.1016/j.yqres.2010.08.014.
Jaccard, S.L., Galbraith, E.D., 2013. Direct ventilation of the North Pacific did not reach the deep ocean during the last deglaciation. Geophys. Res. Lett. 40, 199–203. https://doi.org/10.1029/2012GL054118.
Jaccard, S.L., Galbraith, E.D., Martínez-García, A., Anderson, R.F., 2016. Covariation of deep Southern Ocean oxygenation and atmospheric CO2 through the last ice age. Nature 530, 207–210. https://doi.org/10.1038/nature16514.
Jaccard, S.L., Galbraith, E.D., Sigman, D.M., Haug, G.H., Francois, R., Pedersen, T.F., Dulski, P., Thierstein, H.R., 2009. Subarctic Pacific evidence for a glacial deepening of the oceanic respired carbon pool. Earth Planet Sci. Lett. 277, 156–165. https://doi.org/10.1016/j.epsl.2008.10.017.
Jacobel, A.W., Anderson, R.F., Jaccard, S.L., McManus, J.F., Pavia, F.J., Winckler, G., 2020. Deep Pacific storage of respired carbon during the last ice age: perspectives from bottom water oxygen reconstructions. Quat. Sci. Rev. 230, 106065 https://doi.org/10.1016/j.quascirev.2019.106065.
Jan, S., Yang, Y.J., Wang, J., Mensah, V., Kuo, T.-H., Chiou, M.-D., Chern, C.-S., Chang, M.-H., Chien, H., 2015. Large variability of the Kuroshio at 23.75°N east of taiwan. J. Geophys. Res.: Oceans 120, 1825–1840. https://doi.org/10.1002/2014JC010614.
Jian, Z., Wang, P., Saito, Y., Wang, J., 2000. Holocene variability of the Kuroshio current in the Okinawa Trough, northwestern Paci'c ocean. Earth Planet Sci. Lett. 15.
Jørgensen, B.B., Wenzhöfer, F., Egger, M., Glud, R.N., 2022. Sediment oxygen consumption: role in the global marine carbon cycle. Earth Sci. Rev. 228, 103987 https://doi.org/10.1016/j.earscirev.2022.103987.
Jorissen, F.J., de Stigter, H.C., Widmark, J.G.V., 1995. A conceptual model explaining benthic foraminiferal microhabitats. Marine Micro. Selected papers from the Fifth International Symp. Foram. 26, 3–15. https://doi.org/10.1016/0377-8398(95)00047-X.
Jorissen, F.J., Fontanier, C., Thomas, E., 2007. Chapter seven paleoceanographical proxies based on deep-sea benthic foraminiferal assemblage characteristics. In: Hillaire–Marcel, C., De Vernal, A. (Eds.), Developments in Marine Geology, Proxies in Late Cenozoic Paleoceanography. Elsevier, pp. 263–325. https://doi.org/10.1016/S1572-5480(07)01012-3.
Jorissen, F.J., Wittling, I., 1999. Ecological evidence from live–dead comparisons of benthic foraminiferal faunas off Cape Blanc (Northwest Africa). Palaeogeogr. Palaeoclimatol. Palaeoecol. 149, 151–170. https://doi.org/10.1016/S0031-0182(98)00198-9.
Kaiho, K., 1994. Benthic foraminiferal dissolved-oxygen index and dissolved-oxygen levels in the modern ocean. Geology 22, 719–722, 10.1130/0091-7613(1994)022<0719:BFDOIA>2.3.CO;2.
Kao, S.J., Dai, M., Selvaraj, K., Zhai, W., Cai, P., Chen, S.N., Yang, J.Y.T., Liu, J.T., Liu, C.C., Syvitski, J.P.M., 2010. Cyclone-driven deep sea injection of freshwater and heat by hyperpycnal flow in the subtropics. Geophys. Res. Lett. 37 https://doi.org/10.1029/2010GL044893.
Kao, S.J., Dai, M.H., Wei, K.Y., Blair, N.E., Lyons, W.B., 2008. Enhanced supply of fossil organic carbon to the Okinawa Trough since the last deglaciation. Paleoceanography 23. https://doi.org/10.1029/2007PA001440.
Kao, S.-J., Hilton, R.G., Selvaraj, K., Dai, M., Zehetner, F., Huang, J.-C., Hsu, S.-C., Sparkes, R., Liu, J.T., Lee, T.-Y., Yang, J.-Y.T., Galy, A., Xu, X., Hovius, N., 2014. Preservation of terrestrial organic carbon in marine sediments offshore Taiwan: mountain building and atmospheric carbon dioxide sequestration. Earth Surf. Dyn. 2, 127–139. https://doi.org/10.5194/esurf-2-127-2014.
Kao, S.J., Milliman, J.D., 2008. Water and sediment discharge from small mountainous rivers, taiwan: the roles of lithology, episodic events, and human activities. J. Geol. 116, 431–448. https://doi.org/10.1086/590921.
Kawabe, M., Fujio, S., 2010. Pacific ocean circulation based on observation. J. Oceanogr. 66, 389–403. https://doi.org/10.1007/s10872-010-0034-8.
Keigwin, L.D., 1998. Glacial-age hydrography of the far northwest Pacific Ocean. Paleoceanography 13, 323–339. https://doi.org/10.1029/98PA00874.
Keigwin, L.D., Lehman, S.J., 2015. Radiocarbon evidence for a possible abyssal front near 3.1 km in the glacial equatorial Pacific Ocean. Earth Planet Sci. Lett. 425, 93–104. https://doi.org/10.1016/j.epsl.2015.05.025.
Kitazato, H., Shirayama, Y., Nakatsuka, T., Fujiwara, S., Shimanaga, M., Kato, Y., Okada, Y., Kanda, J., Yamaoka, A., Masuzawa, T., Suzuki, K., 2000. Seasonal phytodetritus deposition and responses of bathyal benthic foraminiferal populations in Sagami Bay, Japan: preliminary results from "Project Sagami 1996–1999.". Mar. Micropaleontol. 40, 135–149. https://doi.org/10.1016/S0377-8398(00)00036-0.
Koho, K.A., Langezaal, A.M., van Lith, Y.A., Duijnstee, I.A.P., van der Zwaan, G.J., 2008. The influence of a simulated diatom bloom on deep-sea benthic foraminifera and the activity of bacteria: a mesocosm study. Deep Sea Res. Oceanogr. Res. Pap. 55, 696–719. https://doi.org/10.1016/j.dsr.2008.02.003.
Kranner, M., Harzhauser, M., Beer, C., Auer, G., Piller, W.E., 2022. Calculating dissolved marine oxygen values based on an enhanced Benthic Foraminifera Oxygen Index. Sci. Rep. 12, 1376. https://doi.org/10.1038/s41598-022-05295-8.
Kuhnt, W., Moullade, M., Kaminski, M.A., 1996. Ecological structuring and evolution of deep sea agglutinated foraminifera — a review. Rev. Micropaleontol. 39, 271–281. https://doi.org/10.1016/S0035-1598(96)90119-1.
Kurtarkar, S.R., Kaithwar, A., Saraswat, R., 2024. Response of inner shelf benthic foraminiferal community to different concentrations of dissolved oxygen under laboratory culture experiment. J. Palaeontological Soc. India. https://doi.org/10.1177/05529360241254215.
Lambeck, K., Rouby, H., Purcell, A., Sun, Y., Sambridge, M., 2014. Sea level and global ice volumes from the last glacial maximum to the Holocene. Proc. Natl. Acad. Sci. U.S.A. 111, 15296–15303. https://doi.org/10.1073/pnas.1411762111.
Langlet, D., Baal, C., Geslin, E., Metzger, E., Zuschin, M., Riedel, B., Risgaard-Petersen, N., Stachowitsch, M., Jorissen, F.J., 2014. Foraminiferal species responses

to in situ, experimentally induced anoxia in the Adriatic Sea. Biogeosciences 11, 1775–1797. https://doi.org/10.5194/bg-11-1775-2014.
Legendre, P., Anderson, M.J., 1999. Distance-based redundancy analysis: testing multispecies responses in multifactorial ecological experiments. Ecol. Monogr. 69, 1–24. https://doi.org/10.1890/0012-9615(1999)069[0001:DBRATM]2.0.CO;2.
Lehu, R., Lallemand, S., Hsu, S.-K., Babonneau, N., Ratzov, G., Lin, A.T., Dezileau, L., 2015. Deep-sea sedimentation offshore eastern Taiwan: facies and processes characterization. Mar. Geol. 369, 1–18. https://doi.org/10.1016/j.margeo.2015.05.013.
Lehu, R., Lallemand, S., Ratzov, G., Babonneau, N., Hsu, S.-K., Lin, A.T., Dezileau, L., 2016. An attempt to reconstruct 2700 years of seismicity using deep-sea turbidites offshore eastern Taiwan. Tectonophysics 692, 309–324. https://doi.org/10.1016/j.tecto.2016.04.030.
Lei, Y., Li, T., 2016. Atlas of benthic foraminifera from China seas. In: The Bohai Sea and the Yellow Sea. Springer Geology. Springer Berlin Heidelberg, Berlin, Heidelberg. https://doi.org/10.1007/978-3-662-53878-4.
Lepš, J., Šmilauer, P., 2003. Multivariate Analysis of Ecological Data Using CANOCO. Cambridge university press.
Letelier, R.M., Björkman, K.M., Church, M.J., Hamilton, D.S., Mahowald, N.M., Scanza, R.A., Schneider, N., White, A.E., Karl, D.M., 2019. Climate-driven oscillation of phosphorus and iron limitation in the North pacific subtropical gyre. Proc. Natl. Acad. Sci. U.S.A. 116, 12720–12728. https://doi.org/10.1073/pnas.1900789116.
Levin, L.A., Gage, J.D., 1998. Relationships between oxygen, organic matter and the diversity of bathyal macrofauna. Deep Sea Res. Part II Top. Stud. Oceanogr. 45, 129–163.
Li, C.-F., Chytry, M., Zelený, D., Chen, J.-J., Chen, T.-Y., Chiou, C.-R., Hsia, Y., Liu, H.-Y., Sheng-Zehn, Y., Yeh, C., Wang, J.-C., Yu, C.-F., Lai, Y.-J., Chao, W.-C., Hsieh, C.-F., 2013. Classification of Taiwan forest vegetation. Appl. Veg. Sci. 16, 698–719. https://doi.org/10.1111/avsc.12025.
Li, D., Chiang, T.-L., Kao, S.-J., Hsin, Y.-C., Zheng, L.-W., Yang, J.-Y.T., Hsu, S.-C., Wu, C.-R., Dai, M., 2017. Circulation and oxygenation of the glacial south China sea. J. Asian Earth Sci. 138, 387–398. https://doi.org/10.1016/j.jseaes.2017.02.017.
Li, G., Rashid, H., Zhong, L., Xu, X., Yan, W., Chen, Z., 2018. Changes in deep water oxygenation of the South China sea since the last glacial period. Geophys. Res. Lett. 45, 9058–9066. https://doi.org/10.1029/2018GL078568.
Li, Q., Li, G., Chen, M.-T., Xu, J., Liu, S., Chen, M., 2020. New insights into Kuroshio current evolution since the last deglaciation based on paired organic paleothermometers from the middle Okinawa Trough. Paleoceanogr. Paleoclimatol. 35, e2020PA004140 https://doi.org/10.1029/2020PA004140.
Lim, D., Kim, J., Xu, Z., Jeong, K., Jung, H., 2017. New evidence for Kuroshio inflow and deepwater circulation in the Okinawa Trough, East China Sea: sedimentary mercury variations over the last 20 kyr. Paleoceanography 32, 571–579. https://doi.org/10.1002/2017PA003116.
Lin, Y.-S., Wei, K.-Y., Lin, I.-T., Yu, P.-S., Chiang, H.-W., Chen, C.-Y., Shen, C.-C., Mii, H.-S., Chen, Y.-G., 2006. The Holocene Pulleniatina minimum event revisited: geochemical and faunal evidence from the Okinawa Trough and upper reaches of the Kuroshio current. Mar. Micropaleontol. 59, 153–170. https://doi.org/10.1016/j.marmicro.2006.02.003.
Linke, P., Lutze, G.F., 1993. Microhabitat preferences of benthic foraminifera—a static concept or a dynamic adaptation to optimize food acquisition? Mar. Micropaleontol. 20, 215–234. https://doi.org/10.1016/0377-8398(93)90034-U.
Locarnini, M.M., Mishonov, A.V., Baranova, O.K., Boyer, T.P., Zweng, M.M., Garcia, H.E., Seidov, D., Weathers, K., Paver, C., Smolyar, I., 2018. World ocean atlas 2018. Temperature 1.
Loeblich Jr, A.R., Tappan, H., 1988. Foraminiferal Genera and Their Classification, first ed. Springer US.
Lu, W., Rickaby, R.E.M., Hoogakker, B.A.A., Rathburn, A.E., Burkett, A.M., Dickson, A.J., Martínez-Méndez, G., Hillenbrand, C.-D., Zhou, X., Thomas, E., Lu, Z., 2020. I/Ca in epifaunal benthic foraminifera: a semi-quantitative proxy for bottom water oxygen in a multi-proxy compilation for glacial ocean deoxygenation. Earth Planet Sci. Lett. 533, 116055 https://doi.org/10.1016/j.epsl.2019.116055.
Lutze, G.F., Thiel, H., 1989. Epibenthic foraminifera from elevated microhabitats; Cibicidoides wuellerstorfi and Planulina ariminensis. J. Foraminifer. Res. 19, 153–158. https://doi.org/10.2113/gsjfr.19.2.153.
Lynch-Stieglitz, J., 2017. The atlantic meridional overturning circulation and abrupt climate change. Ann. Rev. Mar. Sci 9, 83–104. https://doi.org/10.1146/annurev-marine-010816-060415.
Lynch-Stieglitz, J., Adkins, J.F., Curry, W.B., Dokken, T., Hall, I.R., Herguera, J.C., Hirschi, J.J.-M., Ivanova, E.V., Kissel, C., Marchal, O., Marchitto, T.M., McCave, I.N., McManus, J.F., Mulitza, S., Ninnemann, U., Peeters, F., Yu, E.-F., Zahn, R., 2007. Atlantic meridional overturning circulation during the last glacial maximum. Science 316, 66–69. https://doi.org/10.1126/science.1137127.
Mackensen, A., Schmiedl, G., Harloff, J., Giese, M., 1995. Deep-Sea foraminifera in the South Atlantic ocean: ecology and assemblage generation. Micropaleontology 41, 342–358. https://doi.org/10.2307/1485808.
Mahowald, N.M., Baker, A.R., Bergametti, G., Brooks, N., Duce, R.A., Jickells, T.D., Kubilay, N., Prospero, J.M., Tegen, I., 2005. Atmospheric global dust cycle and iron inputs to the ocean. Global Biogeochem. Cycles 19. https://doi.org/10.1029/2004GB002402.
Matsumoto, K., Oba, T., Lynch-Stieglitz, J., Yamamoto, H., 2002. Interior hydrography and circulation of the glacial Pacific Ocean. Quat. Sci. Rev. 21, 1693–1704. https://doi.org/10.1016/S0277-3791(01)00142-1.
Max, L., Lembke-Jene, L., Riethdorf, J.-R., Tiedemann, R., Nürnberg, D., Kühn, H., Mackensen, A., 2014. Pulses of enhanced North Pacific intermediate water ventilation from the Okhotsk Sea and bering Sea during the last deglaciation. Clim. Past 10, 591–605. https://doi.org/10.5194/cp-10-591-2014.
Mazumder, A., Nigam, R., 2014. Bathymetric preference of four major genera of rectilinear benthic foraminifera within oxygen minimum zone in Arabian Sea off central west coast of India. J. Earth Syst. Sci. 123, 633–639. https://doi.org/10.1007/s12040-014-0419-y.
McGann, M., Alexander, C.R., Bay, S.M., 2003. Response of benthic foraminifers to sewage discharge and remediation in Santa Monica Bay, California. Marine Environmental Research, Integrated Assessment of an Urban Water Body: Santa Monica Bay, California 56, 299–342. https://doi.org/10.1016/S0141-1136(02)00336-7.
McGee, D., Moreno-Chamarro, E., Green, B., Marshall, J., Galbraith, E., Bradtmiller, L., 2018. Hemispherically asymmetric trade wind changes as signatures of past ITCZ shifts. Quat. Sci. Rev. 180, 214–228. https://doi.org/10.1016/j.quascirev.2017.11.020.
McManus, J.F., Francois, R., Gherardi, J.-M., Keigwin, L.D., Brown-Leger, S., 2004a. Collapse and rapid resumption of Atlantic meridional circulation linked to deglacial climate changes. Nature 428, 834–837. https://doi.org/10.1038/nature02494.
McManus, J.F., Francois, R., Gherardi, J.-M., Keigwin, L.D., Brown-Leger, S., 2004b. Collapse and rapid resumption of Atlantic meridional circulation linked to deglacial climate changes. Nature 428, 834–837. https://doi.org/10.1038/nature02494.
Meinhold, G., 2010. Rutile and its applications in earth sciences. Earth Sci. Rev. 102, 1–28. https://doi.org/10.1016/j.earscirev.2010.06.001.
Menviel, L., Yu, J., Joos, F., Mouchet, A., Meissner, K.J., England, M.H., 2017. Poorly ventilated deep ocean at the Last Glacial Maximum inferred from carbon isotopes: a data-model comparison study. Paleoceanography 32, 2–17. https://doi.org/10.1002/2016PA003024.
Menviel, L.C., Spence, P., Skinner, L.C., Tachikawa, K., Friedrich, T., Missiaen, L., Yu, J., 2020. Enhanced mid-depth southward transport in the northeast atlantic at the last glacial maximum despite a weaker AMOC. Paleoceanogr. Paleoclimatol. 35, e2019PA003793 https://doi.org/10.1029/2019PA003793.
Milliman, J.D., Farnsworth, K.L., 2011. River Discharge to the Coastal Ocean: A Global Synthesis. Cambridge University Press, Cambridge. https://doi.org/10.1017/CBO9780511781247.
Milliman, J.D., Syvitski, J.P.M., 1992. Geomorphic/tectonic control of sediment discharge to the ocean: the importance of small mountainous rivers. J. Geol. 100, 525–544. https://doi.org/10.1086/629606.
Mix, A.C., Bard, E., Schneider, R., 2001. Environmental processes of the ice age: land, oceans, glaciers (EPILOG). Quat. Sci. Rev. 20, 627–657. https://doi.org/10.1016/S0277-3791(00)00145-1.
Mojtahid, M., Jorissen, F., Lansard, B., Fontanier, C., Bombled, B., Rabouille, C., 2009. Spatial distribution of live benthic foraminifera in the Rhône prodelta: faunal response to a continental–marine organic matter gradient. Mar. Micropaleontol. 70, 177–200. https://doi.org/10.1016/j.marmicro.2008.12.006.
Murgese, D.S., De Deckker, P., 2005. The distribution of deep-sea benthic foraminifera in core tops from the eastern Indian Ocean. Mar. Micropaleontol. 56, 25–49. https://doi.org/10.1016/j.marmicro.2005.03.005.
Murray, J.W., 2006. Ecology and Applications of Benthic Foraminifera. Cambridge University Press, Cambridge. https://doi.org/10.1017/CBO9780511535529.
Naeher, S., Gilli, A., North, R.P., Hamann, Y., Schubert, C.J., 2013. Tracing bottom water oxygenation with sedimentary Mn/Fe ratios in Lake Zurich, Switzerland. Chem. Geol. 352, 125–133. https://doi.org/10.1016/j.chemgeo.2013.06.006.
Nomaki, H., Heinz, P., Nakatsuka, T., Shimanaga, M., Ohkouchi, N., Ogawa, N., Kogure, K., Ikemoto, E., Kitazato, H., 2006. Different ingestion patterns of 13C-labeled bacteria and algae by deep-sea benthic foraminifera. Mar. Ecol. Prog. Ser. 310, 95–108. https://doi.org/10.3354/meps310095.
Nunes, M., Alves Martins, M.V., Frontalini, F., Bouchet, V.M.P., Francescangeli, F., Hohenegger, J., Figueira, R., Senez-Mello, T.M., Louzada Castelo, W.F., Damasceno, F.L., Laut, L., Duleba, W., Mello e Sousa, S.H. de, Antonioli, L., Geraldes, M.C., 2023. Inferring the ecological quality status based on living benthic foraminiferal indices in transitional areas of the Guanabara bay (SE Brazil). Environ. Pollut. 320, 121003 https://doi.org/10.1016/j.envpol.2023.121003.
Ohga, T., Kitazato, H., 1997. Seasonal changes in bathyal foraminiferal populations in response to the flux of organic matter (Sagami Bay, Japan). Terra. Nova 9, 33–37. https://doi.org/10.1046/j.1365-3121.1997.d01-6.x.
Ohkushi, K., Hata, M., Nemoto, N., 2018. Response of deep-sea benthic foraminifera to paleoproductivity changes on the shatsky rise in the northwestern Pacific Ocean over the last 187 kyr. Paleontol. Res. https://doi.org/10.2517/2017PR027.
Ohkushi, K., Itaki, T., Nemoto, N., 2003. Last glacial–holocene change in intermediate-water ventilation in the northwestern pacific. Quat. Sci. Rev. 22, 1477–1484. https://doi.org/10.1016/S0277-3791(03)00082-9.
Ohkushi, K., Kennett, J.P., Zeleski, C.M., Moffitt, S.E., Hill, T.M., Robert, C., Beaufort, L., Behl, R.J., 2013. Quantified intermediate water oxygenation history of the NE Pacific: a new benthic foraminiferal record from Santa Barbara basin. Paleoceanography 28, 453–467. https://doi.org/10.1002/palo.20043.
Ohkushi, K., Natori, H., 2001. Living benthic foraminifera of the hess rise and suiko seamount, central North Pacific. Deep Sea Res. Oceanogr. Res. Pap. 48, 1309–1324. https://doi.org/10.1016/S0967-0637(00)00081-9.
Okazaki, Y., Kimoto, K., Asahi, H., Sato, M., Nakamura, Y., Harada, N., 2014. Glacial to deglacial ventilation and productivity changes in the southern Okhotsk Sea. Palaeogeogr. Palaeoclimatol. Palaeoecol. 395, 53–66. https://doi.org/10.1016/j.palaeo.2013.12.013.
Okazaki, Y., Sagawa, T., Asahi, H., Horikawa, K., Onodera, J., 2012. Ventilation changes in the western North Pacific since the last glacial period. Clim. Past 8, 17–24. https://doi.org/10.5194/cp-8-17-2012.
Okazaki, Y., Timmermann, A., Menviel, L., Harada, N., Abe-Ouchi, A., Chikamoto, M.O., Mouchet, A., Asahi, H., 2010. Deepwater Formation in the North pacific during the

last glacial termination. Science 329, 200–204. https://doi.org/10.1126/science.1190612.
Okumura, Y.M., Deser, C., Hu, A., Timmermann, A., Xie, S.-P., 2009. North pacific climate response to freshwater forcing in the subarctic North atlantic: oceanic and atmospheric pathways. J. Clim. 22, 1424–1445. https://doi.org/10.1175/2008JCLI2511.1.
Ovsepyan, E., Ivanova, E., Tetard, M., Max, L., Tiedemann, R., 2021. Intermediate- and deep-water oxygenation history in the subarctic North Pacific during the last deglacial period. Front. Earth Sci. 9, 638069 https://doi.org/10.3389/feart.2021.638069.
Palmer, H.M., Hill, T.M., Roopnarine, P.D., Myhre, S.E., Reyes, K.R., Donnenfield, J.T., 2020. Southern California margin benthic foraminiferal assemblages record recent centennial-scale changes in oxygen minimum zone. Biogeosciences 17, 2923–2937. https://doi.org/10.5194/bg-17-2923-2020.
Parker, W.C., Arnold, A.J., 1999. Quantitative methods of data analysis in foraminiferal ecology. In: Modern Foraminifera. Springer, Netherlands, Dordrecht, pp. 71–89. https://doi.org/10.1007/0-306-48104-9_5.
Polonia, A., Melis, R., Galli, P., Colizza, E., Insinga, D.D., Gasperini, L., 2023. Large earthquakes along slow converging plate margins: calabrian Arc paleoseismicity based on the submarine turbidite record. Geosci. Front. 14, 101612 https://doi.org/10.1016/j.gsf.2023.101612.
Prospero, J.M., 1990. Mineral-aerosol transport to the North atlantic and North Pacific: the impact of african and asian sources. In: Knap, A.H., Kaiser, M.-S., Kaiser, M.-S. (Eds.), The Long-Range Atmospheric Transport of Natural and Contaminant Substances. Springer, Netherlands, Dordrecht, pp. 59–86. https://doi.org/10.1007/978-94-009-0503-0_4.
Qu, T., Lukas, R., 2003. The bifurcation of the North equatorial current in the pacific. J. Phys. Oceanogr. 33, 5–18. https://doi.org/10.1175/1520-0485(2003)033<0005:TBOTNE>2.0.CO;2.
Rae, J.W.B., Gray, W.R., Wills, R.C.J., Eisenman, I., Fitzhugh, B., Fotheringham, M., Littley, E.F.M., Rafter, P.A., Rees-Owen, R., Ridgwell, A., Taylor, B., Burke, A., 2020. Overturning circulation, nutrient limitation, and warming in the Glacial North Pacific. Sci. Adv. 6, eabd1654 https://doi.org/10.1126/sciadv.abd1654.
Rae, J.W.B., Sarnthein, M., Foster, G.L., Ridgwell, A., Grootes, P.M., Elliott, T., 2014. Deep water formation in the North Pacific and deglacial CO2 rise. Paleoceanography 29, 645–667. https://doi.org/10.1002/2013PA002570.
Rafter, P.A., Gray, W.R., Hines, S.K.V., Burke, A., Costa, K.M., Gottschalk, J., Hain, M.P., Rae, J.W.B., Southon, J.R., Walczak, M.H., Yu, J., Adkins, J.F., DeVries, T., 2022. Global reorganization of deep-sea circulation and carbon storage after the last ice age. Sci. Adv. 8, eabq5434 https://doi.org/10.1126/sciadv.abq5434.
Ramsey, C.B., 2008. Deposition models for chronological records. Quaternary Science Reviews, INTegration of Ice-core, Marine and Terrestrial records (INTIMATE): Refining the record of the Last Glacial-Interglacial Transition 27, 42–60. https://doi.org/10.1016/j.quascirev.2007.01.019.
Ranju, R., Joydas, T.V., Damodaran, R., 2022. Unilocular calcareous benthic foraminifera from the deep-sea sediments of the Bay of Bengal. Regional Studies in Marine Science 55, 102558. https://doi.org/10.1016/j.rsma.2022.102558.
Rathburn, A.E., Corliss, B.H., 1994. The ecology of living (stained) deep-sea benthic foraminifera from the Sulu Sea. Paleoceanography 9, 87–150. https://doi.org/10.1029/93PA02327.
Rathburn, A.E., Corliss, B.H., Tappa, K.D., Lohmann, K.C., 1996. Comparisons of the ecology and stable isotopic compositions of living (stained) benthic foraminifera from the Sulu and South China Seas. Deep Sea Res. Oceanogr. Res. Pap. 43, 1617–1646. https://doi.org/10.1016/S0967-0637(96)00071-4.
Ratzov, G., Revel, M., Chaumulon, A., Babonneau, N., Hsu, S.-K., Lallemand, S., Cattaneo, A., 2023. Enregistrement mixte paléosismique et paléoclimatique à haute résolution, révélé par les turbidites à l'est de Taiwan au cours des derniers 2000 ans.
Resentini, A., Goren, L., Castelltort, S., Garzanti, E., 2017. Partitioning sediment flux by provenance and tracing erosion patterns in Taiwan. J. Geophys. Res.: Earth Surf. 122, 1430–1454. https://doi.org/10.1002/2016JF004026.
Ricotta, C., Pavoine, S., 2022. A new parametric measure of functional dissimilarity: bridging the gap between the Bray-Curtis dissimilarity and the Euclidean distance. Ecol. Model. 466, 109880 https://doi.org/10.1016/j.ecolmodel.2022.109880.
Ruddiman, W.F., 2001. Earth's Climate: Past and Future. Macmillan.
Sanchez Goñi, M.F., Harrison, S.P., 2010. Millennial-scale climate variability and vegetation changes during the Last Glacial: concepts and terminology. Quat. Sci. Rev. 29, 2823–2827. https://doi.org/10.1016/j.quascirev.2009.11.014.
Schlitzer, R., 2022. Ocean Data View.
Schmiedl, G., de Bovée, F., Buscail, R., Charrière, B., Hemleben, C., Medernach, L., Picon, P., 2000. Trophic control of benthic foraminiferal abundance and microhabitat in the bathyal Gulf of Lions, western Mediterranean Sea. Mar. Micropaleontol. 40, 167–188. https://doi.org/10.1016/S0377-8398(00)00038-4.
Schmiedl, G., Mackensen, A., Müller, P.J., 1997. Recent benthic foraminifera from the eastern South Atlantic Ocean: dependence on food supply and water masses. Mar. Micropaleontol. 32, 249–287. https://doi.org/10.1016/S0377-8398(97)00023-6.
Schonfeld, J., 2001. Benthic foraminifera and pore-water oxygen profiles: a re-assessment of species boundary conditions at the western iberian margin. J. Foraminifer. Res. 31, 86–107. https://doi.org/10.2113/0310086.
Sen Gupta, B.K., 1999. Modern Foraminifera. Springer.
Sharon, S., Belanger, C.L., 2022. Placing North Pacific paleo-oxygenation records on a common scale using multivariate analysis of benthic foraminiferal assemblages. Quat. Sci. Rev. 280, 107412 https://doi.org/10.1016/j.quascirev.2022.107412.
Shibahara, A., Ohkushi, K., Kennett, J.P., Ikehara, K., 2007. Late Quaternary changes in intermediate water oxygenation and oxygen minimum zone, northern Japan: a benthic foraminiferal perspective. Paleoceanography 22. https://doi.org/10.1029/2005PA001234.
Siegel, D.A., DeVries, T., Cetinić, I., Bisson, K.M., 2023. Quantifying the oceanocean's biological pump and its carbon cycle impacts on global scales. Ann. Rev. Mar. Sci 15, 329–356. https://doi.org/10.1146/annurev-marine-040722-115226.
Sigman, D.M., Fripiat, F., Studer, A.S., Kemeny, P.C., Martínez-García, A., Hain, M.P., Ai, X., Wang, X., Ren, H., Haug, G.H., 2021. The Southern Ocean during the ice ages: a review of the Antarctic surface isolation hypothesis, with comparison to the North Pacific. Quat. Sci. Rev. 254, 106732 https://doi.org/10.1016/j.quascirev.2020.106732.
Sigman, D.M., Jaccard, S.L., Haug, G.H., 2004. Polar ocean stratification in a cold climate. Nature 428, 59–63. https://doi.org/10.1038/nature02357.
Skinner, L.C., Fallon, S., Waelbroeck, C., Michel, E., Barker, S., 2010. Ventilation of the deep Southern Ocean and deglacial CO2 rise. Science 328, 1147–1151.
Smith, A.J., Gallagher, S.J., 2003. The Recent foraminifera and facies of the Bass Canyon: a temperate submarine canyon in Gippsland, Australia. J. Micropalaeontol. 22, 63–83. https://doi.org/10.1144/jm.22.1.63.
Smith, A.J., Gallagher, S.J., Wallace, M., Holdgate, G., Daniels, J., Keene, J., 2001. The Recent temperate foraminiferal biofacies of the Gippsland Shelf: an analogue for Neogene environmental analyses in southeastern Australia. J. Micropalaeontol. 20, 127–142. https://doi.org/10.1144/jm.20.2.127.
Sousa, S.H.M., Passos, R.F., Fukumoto, M., da Silveira, I.C.A., Figueira, R.C.L., Koutsoukos, E.A.M., de Mahiques, M.M., Rezende, C.E., 2006. Mid-lower bathyal benthic foraminifera of the Campos Basin, Southeastern Brazilian margin: biotopes and controlling ecological factors. Marine Micropal. Forami. Environmental Micropa. 61, 40–57. https://doi.org/10.1016/j.marmicro.2006.05.003.
Sousa, S.H.M., Yamashita, C., Vicente, T.M., Mendes, R.N.M., Licari, L., Alves Martins, M. V., Kim, B.S.M., Millo, C., Carreira, R., Montoya-Montes, I., Kaminski, M.A., Mahiques, M.M., 2024. Living benthic foraminifera from Almirante Câmara and Grussaí canyons and adjacent slope areas (Campos Basin, Southwest Atlantic): response to trophic and hydrodynamic conditions. Deep Sea Res. Oceanogr. Res. Pap. 204, 104231 https://doi.org/10.1016/j.dsr.2024.104231.
Stager, J.C., Ryves, D.B., Chase, B.M., Pausata, F.S., 2011. Catastrophic drought in the Afro-Asian monsoon region during Heinrich event 1. Science 331, 1299–1302.
Steer, P., Jeandet, L., Cubas, N., Marc, O., Meunier, P., Simoes, M., Cattin, R., Shyu, J.B. H., Mouyen, M., Liang, W.-T., Theunissen, T., Chiang, S.-H., Hovius, N., 2020. Earthquake statistics changed by typhoon-driven erosion. Sci. Rep. 10, 10899 https://doi.org/10.1038/s41598-020-67865-y.
Steinke, S., Mohtadi, M., Groeneveld, J., Lin, L.-C., Löwemark, L., Chen, M.-T., Rendle-Bühring, R., 2010. Reconstructing the southern south China sea upper water column structure since the last glacial maximum: implications for the East asian winter monsoon development. Paleoceanography 25, PA2219. https://doi.org/10.1029/2009PA001850.
Sun, Y., Clemens, S.C., Morrill, C., Lin, X., Wang, X., An, Z., 2012. Influence of Atlantic meridional overturning circulation on the East Asian winter monsoon. Nat. Geosci. 5, 46–49. https://doi.org/10.1038/ngeo1326.
Symphonia, T., Senthil, N., 2019. Taxonomic notes on recent foraminifera from the continental shelf-slope region of southwestern bay of bengal, east coast of India. Palaeontol. Electron. https://doi.org/10.26879/811.
Szarek, R., Nomaki, H., Kitazato, H., 2007. Living deep-sea benthic foraminifera from the warm and oxygen-depleted environment of the Sulu Sea. Deep-Sea Res. Part II: Topical Studies in Oceanography, Biogeochemistry and Biodiversity in the Sulu Sea 54, 145–176. https://doi.org/10.1016/j.dsr2.2006.02.017.
Talley, L.D., Pickard, G.L., Emery, W.J. (Eds.), 2011. Descriptive Physical Oceanography: an Introduction, sixth ed. Academic Press, Amsterdam ; Boston.
Talling, P.J., Hage, S., Baker, M.L., Bianchi, T.S., Hilton, R.G., Maier, K.L., 2024. The global turbidity current pump and its implications for organic carbon cycling. Ann. Rev. Mar. Sci 16, 105–133. https://doi.org/10.1146/annurev-marine-032223-103626.
Tetard, M., Licari, L., Beaufort, L., 2017. Oxygen history off Baja California over the last 80 kyr: a new foraminiferal-based record. Paleoceanography 32, 246–264. https://doi.org/10.1002/2016PA003034.
Tetard, M., Licari, L., Ovsepyan, E., Tachikawa, K., Beaufort, L., 2021. Toward a global calibration for quantifying past oxygenation in oxygen minimum zones using benthic Foraminifera. Biogeosciences 18, 2827–2841. https://doi.org/10.5194/bg-18-2827-2021.
Uchimura, H., Nishi, H., Takashima, R., Kuroyanagi, A., Yamamoto, Y., Kutterolf, S., 2017. Distribution of recent benthic foraminifera off western Costa Rica in the eastern equatorial Pacific Ocean. jpal 21, 380–396. https://doi.org/10.2517/2017PR003.
Ujiié, H., Ujiié, Y., 1999. Late quaternary course changes of the Kuroshio current in the Ryukyu Arc region, northwestern Pacific Ocean. Mar. Micropaleontol. 37, 23–40. https://doi.org/10.1016/S0377-8398(99)00010-9.
Ujiié, Y., Ujiié, H., Taira, A., Nakamura, T., Oguri, K., 2003. Spatial and temporal variability of surface water in the Kuroshio source region, Pacific Ocean, over the past 21,000 years: evidence from planktonic foraminifera. Mar. Micropaleontol. 49, 335–364. https://doi.org/10.1016/S0377-8398(03)00062-8.
Van der Zwaan, G., Duijnstee, ab I., Den Dulk, M., Ernst, S., Jannink, N., Kouwenhoven, T., 1999. Benthic foraminifers: proxies or problems?: a review of paleocological concepts. Earth Sci. Rev. 46, 213–236.
Vats, N., Singh, R.K., Das, M., Holbourn, A., Gupta, A.K., Gallagher, S.J., Pandey, D.K., 2021. Linkages between east China sea deep-sea oxygenation and variability in the East asian summer monsoon and Kuroshio current over the last 400,000 years. Paleoceanogr. Paleoclimatol. 36, e2021PA004261 https://doi.org/10.1029/2021PA004261.
Vicente, T.M., Yamashita, C., Sousa, S.H., de, M. e, Ciotti, A.M., 2021. Evaluation of the relationship between biomass of living (stained) benthic foraminifera and particulate organic matter vertical flux in an oligotrophic region, Campos Basin, southeastern

Brazilian continental margin. J. Sea Res. 176, 102110 https://doi.org/10.1016/j.seares.2021.102110.
Wagner, J.D.M., Cole, J.E., Beck, J.W., Patchett, P.J., Henderson, G.M., Barnett, H.R., 2010. Moisture variability in the southwestern United States linked to abrupt glacial climate change. Nat. Geosci. 3, 110–113. https://doi.org/10.1038/ngeo707.
Walker, M.J.C., Berkelhammer, M., Björck, S., Cwynar, L.C., Fisher, D.A., Long, A.J., Lowe, J.J., Newnham, R.M., Rasmussen, S.O., Weiss, H., 2012. Formal subdivision of the Holocene series/epoch: a discussion paper by a working group of INTIMATE (integration of ice-core, marine and terrestrial records) and the subcommission on quaternary stratigraphy (international commission on stratigraphy). J. Quat. Sci. 27, 649–659. https://doi.org/10.1002/jqs.2565.
Wan, S., Sun, Y., Nagashima, K., 2020. Asian dust from land to sea: processes, history and effect from modern observation to geological records. Geol. Mag. 157, 701–706. https://doi.org/10.1017/S0016756820000333.
Wang, B.-S., Ho, T.-Y., 2020. Aerosol Fe cycling in the surface water of the Northwestern Pacific ocean. Prog. Oceanogr. 183, 102291 https://doi.org/10.1016/j.pocean.2020.102291.
Wang, L.-C., 2024. Subtropical montane vegetation dynamics in response to Holocene climate change in central Taiwan. Veg. Hist. Archaeobotany. https://doi.org/10.1007/s00334-024-00988-8.
Wang, L.-C., Behling, H., Lee, T.-Q., Li, H.-C., Huh, C.-A., Shiau, L.-J., Chang, Y.-P., 2014. Late Holocene environmental reconstructions and their implications on flood events, typhoon, and agricultural activities in NE Taiwan. Clim. Past 10, 1857–1869. https://doi.org/10.5194/cp-10-1857-2014.
Wang, L.-C., Chou, Y.-M., Chen, H.-F., Chang, Y.-P., Chiang, H.-W., Yang, T.-N., Shiau, L.-J., Chen, Y.-G., 2022. Paleolimnological evidence for lacustrine environmental evolution and paleo-typhoon records during the late Holocene in eastern Taiwan. J. Paleolimnol. 68, 7–23. https://doi.org/10.1007/s10933-020-00153-x.
Wang, Y., Costa, K.M., Lu, W., Hines, S.K.V., Nielsen, S.G., 2024. Global oceanic oxygenation controlled by the Southern Ocean through the last deglaciation. Sci. Adv. 10, eadk2506 https://doi.org/10.1126/sciadv.adk2506.
Ward, J.H., 1963. Hierarchical grouping to optimize an objective function. J. Am. Stat. Assoc. 58, 236–244.
Warren, B.A., 1983. Why is no deep water formed in the North Pacific? J. Mar. Res. 41, 327–347.
Watson, A.J., Vallis, G.K., Nikurashin, M., 2015. Southern Ocean buoyancy forcing of ocean ventilation and glacial atmospheric CO2. Nat. Geosci. 8, 861–864. https://doi.org/10.1038/ngeo2538.
Wen, Z., Browning, T.J., Cai, Y., Dai, R., Zhang, R., Du, C., Jiang, R., Lin, W., Liu, X., Cao, Z., Hong, H., Dai, M., Shi, D., 2022. Nutrient regulation of biological nitrogen fixation across the tropical western North Pacific. Sci. Adv. 8, eabl7564. https://doi.org/10.1126/sciadv.abl7564.
Wilson, B., 2013. A guide to 1,000 foraminifera from southwestern Pacific, New Caledonia. J. Foraminifer. Res. 43, 314–315. https://doi.org/10.2113/gsjfr.43.3.314.
Wu, L., Wang, R., Xiao, W., Krijgsman, W., Li, Q., Ge, S., Ma, T., 2018. Late quaternary deep stratification-climate coupling in the Southern Ocean: implications for changes in abyssal carbon storage. G-cubed 19, 379–395. https://doi.org/10.1002/2017GC007250.
Xiang, R., Li, T., Yang, Z., Li, A., Jiang, F., Yan, J., Cao, Q., 2003. Geological records of marine environmental changes in the southern Okinawa Trough. Chin. Sci. Bull. 48, 194–199. https://doi.org/10.1360/03tb9040.
Xiang, R., Sun, Y., Li, T., Oppo, D.W., Chen, M., Zheng, F., 2007. Paleoenvironmental change in the middle Okinawa Trough since the last deglaciation: evidence from the sedimentation rate and planktonic foraminiferal record. Palaeogeogr. Palaeoclimatol. Palaeoecol. 243, 378–393. https://doi.org/10.1016/j.palaeo.2006.08.016.
Xu, X., Oda, M., 1999. Surface-water evolution of the eastern East China Sea during the last 36,000 years. Mar. Geol. 156, 285–304. https://doi.org/10.1016/S0025-3227(98)00183-2.
Xu, Y., Chang, F.-M., Li, T.-G., Li, B.-H., 2021. High-resolution sea surface temperature and salinity dynamics in the northern Okinawa Trough over the last 24 kyr. Palaeoworld 30, 770–785. https://doi.org/10.1016/j.palwor.2020.12.005.
Xu, Z., Li, T., Clift, P.D., Lim, D., Wan, S., Chen, H., Tang, Z., Jiang, F., Xiong, Z., 2015. Quantitative estimates of Asian dust input to the western Philippine Sea in the mid-late Quaternary and its potential significance for paleoenvironment: asian dust input to WPS IN quaternary. G-cubed 16, 3182–3196. https://doi.org/10.1002/2015GC005929.
Xu, Z., Wan, S., Colin, C., Li, T., Clift, P.D., Chang, F., Sun, R., Yu, Z., Lim, D., 2020. Enhanced terrigenous organic matter input and productivity on the western margin of the Western Pacific Warm Pool during the Quaternary sea-level lowstands: forcing mechanisms and implications for the global carbon cycle. Quat. Sci. Rev. 232, 106211 https://doi.org/10.1016/j.quascirev.2020.106211.
Yamashita, C., de Mello e Sousa, S.H., Kaminski, M.A., Alves Martins, M.V., Elmadjian, C. E.L., Nagai, R.H., Yamamoto, N.T., Koutsoukos, E.A.M., Figueira, R.C.L., 2019. Description, distribution and ecology of living *Reophax pyriformis* n. sp. (campos basin, South Atlantic ocean). Rev. Micropaleontol. 64, 100360 https://doi.org/10.1016/j.revmic.2019.06.002.
Yang, Y., Zhang, L., Yi, L., Zhong, F., Lu, Z., Wan, S., Du, Y., Xiang, R., 2023. A contracting intertropical convergence zone during the early Heinrich stadial 1. Nat. Commun. 14, 4695. https://doi.org/10.1038/s41467-023-40377-9.
Yang, Z., Li, T., Lei, Y., Chang, F., Nan, Q., 2020. Vegetation evolution-based hydrological climate history since LGM in southern South China Sea. Mar. Micropaleontol. 156, 101837 https://doi.org/10.1016/j.marmicro.2020.101837.
You, Y., Suginohara, N., Fukasawa, M., Yoritaka, H., Mizuno, K., Kashino, Y., Hartoyo, D., 2003. Transport of North Pacific intermediate water across Japanese WOCE sections. J. Geophys. Res.: Oceans 108. https://doi.org/10.1029/2002JC001662.
Yu, S.-W., Tsai, L.L., Talling, P.J., Lin, A.T., Mii, H.-S., Chung, S.-H., Horng, C.-S., 2017. Sea level and climatic controls on turbidite occurrence for the past 26kyr on the flank of the Gaoping Canyon off SW Taiwan. Mar. Geol. 392, 140–150. https://doi.org/10.1016/j.margeo.2017.08.011.
Yu, Z., Tang, X., Colin, C., Wilson, D.J., Zhou, X., Song, L., Chang, F., Zhang, S., Bassinot, F., Wan, S., 2023. Millennial-scale precipitation variability in the indo-pacific region over the last 40 kyr. Geophys. Res. Lett. 50, e2022GL101646 https://doi.org/10.1029/2022GL101646.
Zarriess, M., Mackensen, A., 2010. The tropical rainbelt and productivity changes off northwest Africa: a 31,000-year high-resolution record. Mar. Micropaleontol. 76, 76–91. https://doi.org/10.1016/j.marmicro.2010.06.001.
Zhang, H., Liu, C., Jin, X., Shi, J., Zhao, S., Jian, Z., 2016. Dynamics of primary productivity in the northern South China Sea over the past 24,000 years: productivity in the South China Sea. G-cubed 17, 4878–4891. https://doi.org/10.1002/2016GC006602.
Zheng, L.-W., Hilton, R.G., Chang, Y.-P., Yang, R.J., Ding, X., Zheng, X., Lee, T.-Y., Lu, H.-J., Lu, J.-T., Lin, Y.-S., Liu, J.T., Kao, S.-J., 2024. Climate-regulation of organic carbon export in erosive mountain settings: a case study from Taiwan since the last glacial maximum. Quat. Sci. Rev. 334, 108687 https://doi.org/10.1016/j.quascirev.2024.108687.
Zhong, Y., Shi, X., Yang, H., Wilson, D.J., Hein, J.R., Kaboth-Bahr, S., Lu, Z., Clift, P.D., Yan, Q., Lohmann, G., Liu, J., González, F.J., Jiang, X., Jiang, Z., Liu, Q., 2022. Humidification of Central Asia and equatorward shifts of westerly winds since the late Pliocene. Commun Earth Environ. 3, 1–9. https://doi.org/10.1038/s43247-022-00604-5.
Ziegler, M., Jilbert, T., de Lange, G.J., Lourens, L.J., Reichart, G.-J., 2008. Bromine counts from XRF scanning as an estimate of the marine organic carbon content of sediment cores. G-cubed 9. https://doi.org/10.1029/2007GC001932.
Zou, J., Chang, Y.-P., Zhu, A., Chen, M.-T., Kandasamy, S., Yang, H., Cui, J., Yu, P.-S., Shi, X., 2021. Sedimentary mercury and antimony revealed orbital-scale dynamics of the Kuroshio Current. Quat. Sci. Rev. 265, 107051 https://doi.org/10.1016/j.quascirev.2021.107051.
Zou, J., Shi, X., Zhu, A., Kandasamy, S., Gong, X., Lembke-Jene, L., Chen, M.-T., Wu, Y., Ge, S., Liu, Y., Xue, X., Lohmann, G., Tiedemann, R., 2020. Millennial-scale variations in sedimentary oxygenation in the western subtropical North Pacific and its links to North Atlantic climate. Clim. Past 16, 387–407. https://doi.org/10.5194/cp-16-387-2020.
Zweng, M., Reagan, J., Seidov, D., Boyer, T., Locarnini, M., Garcia, H., Mishonov, A., Baranova, O., Weathers, K., Paver, C., Smolyar, I., 2019. World Ocean atlas 2018. Salinity 2.